UPPSALA
UNIVERSITET

Digital Comprehensive Summaries of Uppsala Dissertations from the Faculty of Science and Technology 658

Development of Electroacoustic Sensors for Biomolecular Interaction Analysis

HENRIK ANDERSON

ACTA
UNIVERSITATIS
UPSALIENSIS
UPPSALA
2009

ISSN 1651-6214
ISBN 978-91-554-7572-7
urn:nbn:se:uu:diva-107211

Dissertation presented at Uppsala University to be publicly examined in Å80101, Ångströmlaboratoriet, Lägerhyddsvägen 1, Uppsala, Friday, September 11, 2009 at 09:30 for the degree of Doctor of Philosophy. The examination will be conducted in English.

Abstract
Anderson, H. 2009. Development of Electroacoustic Sensors for Biomolecular Interaction Analysis. Acta Universitatis Upsaliensis. *Digital Comprehensive Summaries of Uppsala Dissertations from the Faculty of Science and Technology* 658. 70 pp. Uppsala.
ISBN 978-91-554-7572-7.

Biomolecular interaction analysis to determine the kinetics and affinity between interacting partners is important for the fundamental understanding of biology, as well as for the development of new pharmaceutical substances. A quartz crystal microbalance instrument suitable for kinetics and affinity analyses of interaction events was developed. The functionality of the sensor system was demonstrated by development of an assay for relative affinity determination of lectin-carbohydrate interactions.

Sensor surfaces allowing for effective immobilization of one interacting partner is a key functionality of a biosensor. Here, three different surfaces and immobilization methods were studied. First, optimized preparation conditions for sensor surfaces based on carboxyl-terminated self assembled monolayers were developed and were demonstrated to provide highly functional biosensor surfaces with low non-specific binding. Second, a method allowing for immobilization of very acidic biomolecules based on the use of an electric field was developed and evaluated. The electric field made it possible to immobilize the highly acidic C-peptide on a carboxylated surface. Third, a method for antibody immobilization on a carboxyl surface was optimized and the influence of immobilization pH on the immobilization level and antigen binding capacity was thoroughly assessed. The method showed high reproducibility for a set of antibodies and allowed for antibody immobilization also at low pH.

Three broadly different strategies to increase the sensitivity of electroacoustic sensors were explored. A QCM sensor with small resonator electrodes and reduced flow cell dimensions was demonstrated to improve the mass transport rate to the sensor surface. The use of polymers on QCM sensor surfaces to enhance the sensor response was shown to increase the response of an antibody-antigen model system more than ten-fold. Moreover, the application of high frequency thin film bulk acoustic resonators for biosensing was evaluated with respect to sensing range from the surface. The linear detection range of the thin film resonator was determined to be more than sufficient for biosensor applications involving, for instance, antibody-antigen interactions. Finally, a setup for combined frequency and resistance measurements was developed and was found to provide time resolved data suitable for kinetics determination.

Keywords: biosensor, protein interactions, kinetics, affinity, QCM, quartz crystal microbalance, piezoelectric resonators, dissipation, motional resistance

Henrik Anderson, Solid State Electronics, Box 534, Uppsala University, SE-75121 Uppsala, Sweden

ISSN 1651-6214
ISBN 978-91-554-7572-7
urn:nbn:se:uu:diva-107211 (http://urn.kb.se/resolve?urn=urn:nbn:se:uu:diva-107211)

List of Papers

I Pei, Z., Anderson, H., Aastrup, T., Ramström, O. (2005) Study of real-time lectin–carbohydrate interactions on the surface of a quartz crystal microbalance. *Biosensors & Bioelectronics*, 21: 60–66.

II Myrskog, A., Anderson, H., Ingemarsson, B., Liedberg, B. (2009) Esterification of self-assembled carboxylic acid-terminated thiol monolayers in acid environment: A time dependent study. *Submitted to Langmuir.*

III Melles, E., Anderson, H., Wallinder, D., Shafgat, J., Bergman, T., Aastrup, T., Jörnvall, H. (2005) Electroimmobilization of proinsulin C-peptide to a quartz crystal microbalance sensor chip for protein affinity purification. *Analytical Biochemistry*, 341 (1): 89-93.

IV Anderson, H., Myrskog, A., Ingemarsson, B., Aastrup, T., Pei, Z. (2009) Optimizing immobilization conditions on a two dimensional carboxyl biosensor surface: pH dependence of antibody orientation and antigen binding capacity. *Submitted to Analytical Biochemistry.*

V Anderson, H., Jönsson, M., Vestling, L., Lindberg, U., Aastrup, T. (2007) Quartz crystal microbalance sensor design: I. Experimental study of sensor response and performance. *Sensors and Actuators B Chemical,* 123 (1): 27-34.

VI Jönsson, M., Anderson, H., Lindberg, U., Aastrup, T. (2007) Quartz crystal microbalance biosensor design: II. Simulations of sample transport, *Sensors and Actuators B Chemical,* 123 (1): 21-26.

VII Dunér, G., Anderson, H., Myrskog, A., Hedlund, M., Aastrup, T., Ramström, O. (2008) Surface-confined photopolymerization of pH-responsive Acrylamide/acrylate-Brushes on Polymer Thin Films. *Langmuir*, 24: 7559-7564.

VIII Dunér, G., Anderson, H., Pei, Z., Ingemarsson, B., Aastrup, T., Ramström, O. (2009) Signal Enhancement in Ligand-Receptor Interactions using Dynamic Polymers at Quartz Crystal Microbalance Surfaces. *In manuscript*.

IX Wingqvist, G., Anderson, H., Lennartsson, C., Weissbach, T., Yantchev, V., Lloyd Spetz, A. (2009) On the applicability of high frequency shear mode biosensing in view of thickness limitations set by the film resonance, *Biosensors and Bioelectronics* 24: 3387–3390.

X Anderson, H., Wingqvist, G., Weissbach, T., Wallinder, D., Aastrup, T., Katardjiev, I., Ingemarsson, B. (2009) Systematic investigation of biomolecular interactions using combined frequency and motional resistance measurements. *Submitted to Journal of Molecular Recognition.*

Reprints were made with permission from the respective publishers.

Contribution report

I Major part in development of the experimental setup and surface preparation method. Part in writing.
II Part in experimental planning, evaluation and writing.
III Major part in design of experimental setup, experimental planning, evaluation and part in writing.
IV Major part in experimental work and writing.
V Major part in experimental planning, evaluation and writing. Design of experimental setup.
VI Major part in planning, evaluation and experimental work. Part in writing.
VII Part in experimental planning, evaluation and writing.
VIII Part in experimental planning, evaluation and writing.
IX Part in experimental planning, evaluation and writing.
X All experimental work, major part in evaluation and writing.

Publications not included in this thesis

1. Myrskog, A., Ruželė, Z., Anderson, H., Aastrup, T., Valiokas, R., Liedberg, B. (2009) On the stability of carboxylic acid-terminated self-assembled monolayers: Influence of varying alkyl chain length. *In manuscript.*
2. Pei, Z., Larsson, R., Aastrup, T., Anderson, H., Lehn, J.M., Ramstrom, O. (2006) Quartz crystal microbalance bioaffinity sensor for rapid identification of glycosyldisulfide lectin inhibitors from a dynamic combinatorial library, *Biosensors and Bioelectronics* 22: 42-48.
3. Pei, Z., Aastrup, T., Anderson, H., Ramström, O. (2005) Redox-Responsive and Calcium-Dependent Switching of Glycosyldisulfide Interactions with Concanavalin A. *Biorganic and medicinal chemistry letters*, 15 (11): 2707-2710.
4. Pei, Z., Larsson, R., Aastrup, T., Anderson, H., Ramstrom, O. (2005) Rapid screening of glycosyldisulfide lectin inhibitors from a dynamic combinatorial library, *230th National Meeting of the American-Chemical-Society*, Washington, DC, pp. 77-CARB.
5. Anderson, H., Berggren, K., Lindberg, U., Aastrup, T., Hjertén S. (2005) Molecularly imprinted quartz crystal biosensor for protein detection. *Synthetic Receptors 2005*, Salzburg, Austria, September 07-09.
6. Anderson, H., McEnally, C.S., Pfefferle, L.D. (2000) Experimental study of naphthalene formation pathways in non-premixed methane flames doped with alkylbenzenes, *28th International Symposium on Combustion*, Edinburgh, Scotland, pp. 2577-2583.
7. Anderson, H., Bjorkman, H., Aastrup, T., Mass sensitive chemical sensor. *International patent application (PCT)*, WO2008/132487
8. Aastrup, T., Wallinder, D., Anderson, H., Surface preparation method. *International patent application (PCT),* WO2006045558
9. Aastrup, T., Smith, J., Anderson, H. Piezoelectric resonator, *International patent application (PCT),* WO2004072622.
10. Aastrup, T., Smith, J., Anderson, H. Piezoelectric sensor arrangement, *International patent application (PCT),* WO2004057319'
11. Månsson, P., Anderson, H., Smith, J., Jensen., K., Aastrup, T. *International patent application (PCT),* WO2004001392

Contents

Abbreviations

AB	Antibody
AG	Antigen
BSA	Bovine Serum Albumin
BVD	Butterworth van Dyke
CM Dextan	Carboxy-Methylated Dextran
DNA	Deoxyribonucleic Acid
EDC	1-ethyl-3-[3-dimethylaminopropyl] carbodiimide hydrochloride
Fab	Fragment Antigen Binding
FBAR	Thin Film Bulk Acoustic Resonator
Fc	Fragment Crystallizable
IgG	Immunoglobulin G
HAc	Acetic Acid
HCl	Hydrochloric Acid
HSA	Human Serum Albumin
NHS	N-hydroxy-succinimide
pAAc	Poly Acrylic Acid
PBS	Phosphate Buffered Saline
Q	Quartz Quality factor
QCM	Quartz Crystal Microbalance
QCM-D	Quartz Crystal Microbalance with Dissipation monitoring
RNA	Ribonucleic Acid
SAM	Self Assembled Monolayer
SPR	Surface Plasmon Resonance
Sulfo-NHS	N-hydroxysulfo-succinimide
TSM	Thickness Shear Mode

Preface

This thesis focuses on electroacoustic biosensors for molecular interaction studies. Development of electroacoustic sensors, such as quartz crystal microbalances (QCM) and thin film bulk acoustic resonators (FBAR) for biosensor use, is a multidisciplinary research field. It involves aspects ranging from electronics, mechanics and fluidics to chemistry and molecular biology. The width of the field, and the challenge to become knowledgeable in all these areas, are some reasons why I was attracted to the field in the first place. I was first acquainted with the QCM technology when I started as a development engineer at Biosensor Applications now nine years ago. The interest grew stronger along with more experience and, eventually, led to the founding of Attana AB together with Teodor Aastrup, Jan Smith and Samir Fostock in 2002.

Parallel to the development of Attana AB, in 2003 I was enrolled as an industrial doctorate student at Solid State Electronics, Uppsala University, in Dr. Ulf Lindberg's research group with focus on microstructures and microfluidics. Therefore, this thesis concludes research and development work conducted between 2003 and 2009 at Attana AB and the Ångström Laboratory, Uppsala University. The work has been financed by Attana AB and the Swedish Research Council. Several projects have involved collaborations with research groups at other Swedish universities. Specifically, the Papers I, VII and VIII were made in collaboration with Prof. Olof Ramström's research group at Organic Chemistry, KTH. Paper II is the result of collaboration with Prof. Bo Liedberg at IFM, Linköping University. Paper III was made in collaboration with Prof. Hans Jörnvall, MBB, Karolinska Institute and his colleagues.

The thesis aims at providing an introduction to electroacoustic sensors and QCM (Chapter 2) and to molecular interaction studies (Chapter 3). The results of the appended studies are presented in three chapters, discussing different aspects of biosensing. Chapter 4, Biosensor assays describes several important steps in the development of a biosensor assay based on the study of Paper I. Chapter 5, Surfaces and immobilization, discusses matters regarding immobilization and surface chemistry in view of Papers II-IV. Chapter 6 compiles several different approaches related to increasing the sensitivity or performance of acoustic sensors. Since the work stretches over many years and has been influenced by the development of Attana and its products, as well as by the collaborating research groups, presentation of

data differ in the thesis. Specifically, frequency responses from the early studies were presented as negative responses for binding material to the sensor surface. In most of the later papers, conformity with other biosensor techniques has been preferred and consequently the inversed frequency shift is presented.

Many people have been involved in the work that has resulted in this thesis, and I would like to thank all my coauthors for their respective contributions to the appended papers. Specifically, I would like to express my sincere appreciation to the following people.

Teodor Aastrup, Stellan Hjertén and Ulf Lindberg for providing the opportunity of these doctorate studies, and for inspiring discussions during the early years.

Björn Ingemarsson for thorough, detailed and thoughtful input to the work herein, and for helping me across the finish line.

Ilia Katardjiev for taking me on half way through and helping me finish.

Annica Myrskog for impressive thoroughness and persistence in our joint projects and for help in preparation of this thesis.

Gunilla Wingqvist for fruitful discussions and for challenging me to fill the blanks in my knowledge.

Gunnar Dunér for hard work with the difficult challenges of our joint project.

Mats Jönsson for pulling me along in the early years and making me finish Papers V and VI.

Olof Ramström for a long and productive collaboration resulting in Papers I, VII and VIII of this thesis, and for helpful comments in preparation of Paper IV.

Zhichao Pei for patience and determination when working with the first Attana prototype instrument that resulted in the first publication on the Attana QCM (Paper I), and for his contributions to Paper IV which made that publication possible.

Bo Liedberg for long and fruitful collaboration on sensor surfaces both for product development and in the research work that resulted in Paper II. Daniel Aili and Andréas Larsson for help in various collaborations and for providing a welcoming atmosphere at IFM, Linköping University during my visits there.

Ermias Melles, Hans Jörnvall and their colleagues at MBB, KI for stimulating the development of the novel immobilization strategy presented in Paper III, and for their contributions which enabled that publication.

Daniel Wallinder for enlightening discussions on QCM sensor physics and electronics and for his contributions to Papers III and X. Thomas Weissbach for skilful and persistent experimental work in Paper IX, and for generous assistance with instrument issues in general.

Lena Höjvall and Helena Bonin for helpfully providing sensor surfaces and chemicals to several of these studies, and Lena for inspiring a healthy

and environmentally friendly lifestyle by biking the almost 50 km return trip to work every other day.

Karin Berggren for a positive and cheerful disposition and for help with this thesis.

All Attana colleagues, present and past, for helping out with various matters and for providing a friendly and inspiring work environment.

Johan Bjurström, Ventsislav Yantchev and Marianne Asplund for always being helpful and for always making me feel welcome at the Solid State Electronics department.

Särskilt tack till min och Saras familjer för hjälp och stöd under denna tid, och till mina föräldrar för att ni alltid funnits där för mig.

Slutligen och allra mest tack till min älskade Sara som stått ut med mig under tiden av intensivt skrivande och gett mig möjlighet att slutföra detta. Och för att det inte finns någon bättre stund på dagen än när jag kommer hem på kvällen möts av kramar från Sara, Jonatan och Simon.

Stockholm, 2009-07-30

1 Introduction

Life is, in a molecular sense, the interactions between cells, proteins, nucleic acids and other biomolecules. Everything that we do as humans is governed by interactions occurring in our bodies or at their interfaces. For instance, when we smell something this corresponds to interactions between olfactory receptors in the nose and the chemical trace that defines the sensed smell. A disturbance or malfunction in the normal mode of action of an interaction may cause disease and illness. If certain interactions can be manipulated by introducing a drug, the disease or its symptoms may be reduced. To do this, however, the cascades of interactions need to be known, a suitable target receptor defined and a drug that affects the receptor in an appropriate way found.

One means to study these interactions, and how they are influenced by drug candidates, is biosensors. Biosensors for interaction studies involve immobilization of one binding partner on a sensing surface, and the introduction of a second binding partner in solution over the immobilized molecule on the sensing surface. The sensing surface, or transducer, detects binding to the immobilized binding partner in real-time and thereby allows for reaction rates of biomolecular interactions to be determined.

Various transducer principles can be used, of which optical and acoustic biosensors are most widespread. In terms of optical techniques, several variants exist such as surface plasmon resonance (SPR), resonant wavelength grating and ellipsometry. Quartz crystal microbalance (QCM) is the most commonly used acoustic sensor, although an increased use of surface acoustic wave devices and thin film resonators can be noted. Whereas SPR and similar techniques enable determination of the surface concentration of immobilized or bound species at a given time, the QCM also has the advantage of providing information on the structure and conformation of the molecules on the surface by means of dissipation, amplitude or motional resistance measurements.

The aim of this thesis has been to explore the use of acoustic sensors for biomolecular interaction studies by development of a continuous flow QCM system, together with suitable surface chemistries and analysis methods. Also, the potential for further improvement of acoustic sensing by studies of novel transducer and surface chemistry concepts has been conducted.

2 Quartz Crystal Microbalance

The fundamental transduction principle that QCM relies upon is the piezoelectric effect, which was discovered by Jacques and Pierre Curie in 1880 [1]. In 1959, Sauerbrey showed that the frequency shift of a quartz crystal resonator was proportional to the added mass. This was an important milestone for the use of QCM as a quantitative sensor [2]. The use of QCM in liquids was for a long time considered difficult because of the dampening of the crystal. This was, however, overcome by exposing only one side of the quartz crystal to the liquid by which the crystal resonator could be used for analytical purposes in liquids [3,4]. Another significant contribution to the use of QCM in liquids was made by Kanazawa and Gordon when they developed a model describing the response of a quartz crystal resonator to liquid samples of varying viscosities and densities and also proved this experimentally [5]. One of the first bioanalytical applications of piezoelectric sensors was demonstrated by Thompson, et al. in 1986, when a piezoelectric sensor was used for the detection of binding events between human antibodies and goat anti-human antibodies [6]. In 1993, the relationship between adsorbed mass and frequency shift, for a piezoelectric immunosensor in liquids, was studied by Muratsugu and coworkers [7]. Parallel measurements with radioisotopes showed that the frequency response by adsorption of human serum albumin (HSA) and anti human serum albumin antibody (anti-HSA) was higher than expected from the Sauerbrey equation, although the relationship between frequency response and adsorbed mass was still found to be predominantly linear.

A further step in the advancement of piezoelectric sensors was taken by Rodahl and coworkers in 1995, by the development of a QCM setup for combined frequency and Q-factor measurements [8,9]. The measurement of the Q-factor or dissipation, as it was rebranded, was shown to be useful for studies of protein adsorption and the properties of polymers on surfaces, as well as for studies of DNA demonstrated in subsequent papers. Also, the commercialization initiative that followed these investigations and resulted in the QCM-D technology (Q-Sense AB, Sweden) has greatly expanded the use of QCM within surface and biological sciences.

2.1 Acoustic waves

The quartz crystal microbalance is an acoustic sensor, where an acoustic wave is excited within the material by means of an externally applied electric field. The acoustic waves propagate in the bulk of the crystal and are subsequently reflected at the solid/air interfaces or edges. Thus, any perturbation in the material's properties at these edges (say, mass, etc) results in a perturbation of the reflected wave (amplitude, phase), making the resonator a very sensitive element to external influence.

Acoustic waves that propagate in solids constitute coordinated and time variant displacements of the atoms within the material. In elastic materials, the displacement of atoms gives rise to strain in the material that produces a counteracting force or stress that strives to return the atoms to its equilibrium position [10]. The relationship between stress and strain to a first order of approximation is linear with the coefficients of proportionality being the material's elastic constants, also known as Hooke's law. Acoustic waves are classified depending on their propagation characteristics. For longitudinal waves the displacement of atoms is parallel to the propagation direction whereas shear waves propagate in a direction perpendicular to the displacement direction (see Figure 2.1). In contrast to longitudinal and shear waves that propagate in the bulk of the material, surface acoustic waves are confined to the surface of the material and their amplitude decreases exponentially with increasing distance from the surface.

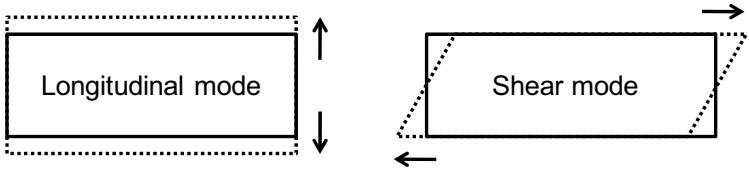

Figure 2.1. Longitudinal and shear mode displacement of a thickness exited substrate

In the context of liquid sensing, acoustic waves that have substantial displacements normal to the sensor surface will radiate compressional waves into the liquid and will thereby suffer excessive damping. Consequently, longitudinal bulk acoustic waves will work poorly in liquid applications. Shear acoustic waves, on the other hand will only generate shear displacement in the liquid with exponentially decaying amplitude since the shear modulus of liquids is zero and thereby most of the wave energy will be confined to the solid material. Examples of suitable waves for liquid sensing are acoustic plate modes, Love waves and thickness shear modes (TSM), the latter mode which being the focus of this thesis.

2.2 Piezoelectric materials

To utilize acoustic waves for sensing there has to be a transduction mechanism that translates changes in the wave properties into electrical signals. This is achieved by use of piezoelectric transducers. A piezoelectric material such as quartz exhibits an electrical polarization when mechanically deformed because of its non-centrosymmetric structure. This means that by application of strain in the material, the distribution of charges within the material changes in a way that leads to a net macroscopic electrical polarization. Conversely, if a potential is applied over the piezoelectric material, it will become mechanically deformed.

A piezoelectric quartz crystal resonator is a precisely cut quartz disk with electrodes concentrically plated on to its faces. The electrodes are used to excite an acoustic wave in the crystal by applying an oscillating potential. The direction of the wave will depend on the crystal orientation in relation to the electrodes, i.e. to the cut angle. To obtain thickness shear mode resonators for liquid sensing purposes the so called AT-cut crystal is predominantly utilized since this cut also has relatively good temperature stability at ambient temperatures.

Acoustic waves in an AT-cut thickness shear resonator will be reflected at the edges of the material. By constructive interference of incident and reflected waves mechanical resonance will be achieved. This will occur at multiples of half a wavelength resulting in a resonance frequency according to,

$$f_N = \frac{N v_s}{2 h_s} \qquad 2.1$$

where N is an integer denoting the resonance harmonic, v_s is the shear wave velocity and h_s is the thickness of the crystal. Accordingly, an AT-cut quartz crystal of 167 µm thickness will have a fundamental resonance frequency of around 10 MHz. In practice, only odd harmonics can be electrically exited. The fundamental resonance frequency and the 3rd harmonic of a thickness shear mode resonator are depicted in Figure 2.2.

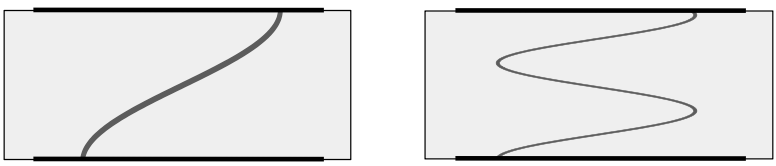

Figure 2.2. The wave propagation in a thickness shear mode resonator electrically excited to the first (left) and third (right) harmonic.

2.3 Equivalent representations

The quartz crystal resonator of a TSM resonator is often described with an equivalent circuit, or Butterworth-van Dyke (BVD) representation, as displayed in Figure 2.3. The representation consists of a branch with a static capacitance (C_0) and a motional branch defining the electromechanical properties of the resonator by serially connected inductance (L_1), resistance (R_1) and capacitance (C_1).

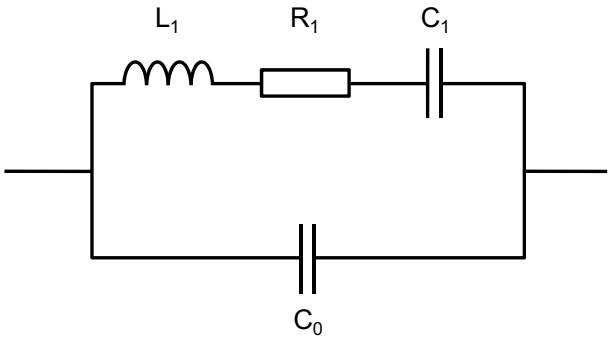

Figure 2.3. Equivalent circuit representation of a quartz crystal resonator.

The series resonance frequency, f_s, is defined as the frequency when the admittance phase angle is zero and the admittance magnitude is close to maximum. This represents the frequency when the motional reactance is zero, whereas the parallel resonance, f_p, is the frequency at which the total reactance is zero[1]. The total admittance of the TSM resonator, Y, and the motional impedance, Z_m, can be written,

$$Y(\omega) = j\omega C_0 + \frac{1}{Z_m} \quad 2.2$$

$$Z_M = R_1 + j\omega L_1 + \frac{1}{j\omega C_1} \quad 2.3$$

The parallel resonance frequency is found also at zero phase angle of the admittance, but close to the minimum of the admittance magnitude as shown in Figure 2.4 below.

[1] Admittance, Y, is the inverse of the impedance, Z, and the reactance is the imaginary part of the impedance. The angular frequency is denoted by ω.

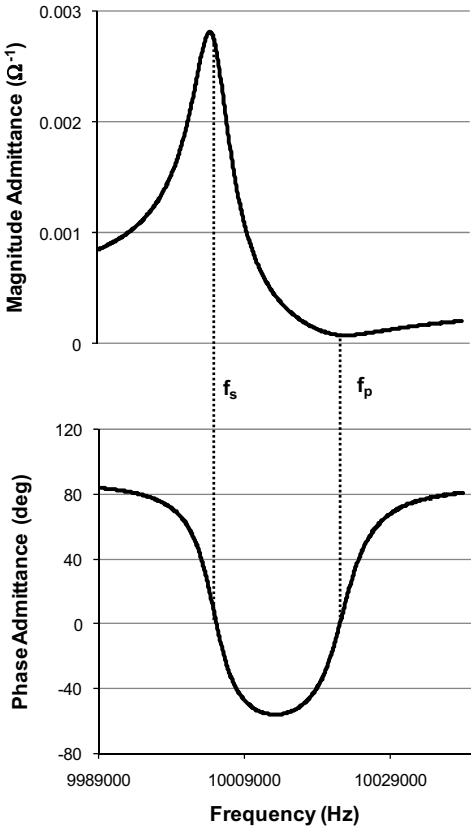

Figure 2.4. Admittance magnitude and phase for a 10 MHz TSM with series and parallel frequencies.

The series resonance could be considered the mechanical resonance of the resonator, and the parallel resonance is more related to the electrical resonance. The separation of the series and parallel resonance defines the electromechanical coupling coefficient which is an indicator of the effectiveness with which a piezoelectric material converts electrical energy into mechanical energy, or converts mechanical energy into electrical energy. Impedance or network analysis allows for determination of both of these frequencies, but for sensor applications when an oscillator circuit is used to determine the resonance frequency, normally only one of the two is obtained.

2.4 Dissipation or resistance measurements

In addition to the resonance frequencies of a TSM resonator, the quality factor (Q-value, Q) can provide supplementary characterization of the resonator. The quality factor Q is a measure of the "sharpness" of the frequency

response and is inversely proportional to the energy loss per cycle of oscillation. It is normally determined from the slope of the phase at a particular frequency. A high quality factor of a resonator means that the resonator looses little energy to the surroundings, resulting in a low noise device and hence high resolution. The inverse of the quality factor is referred to as dissipation, D, and is frequently used for studies of polymer and biological films to gain better understanding of structural events occurring in these films [11].

The information contained in dissipation data, can also be obtained by measurements of the motional resistance. The relationship between serial dissipation, D_s and resistance, R_1, can be expressed in terms of the equivalent circuit as [12]:

$$D_S = \frac{R_1}{2\pi f_s L_1} \tag{2.4}$$

For differential measurements in the frequency bandwidth of a few hundreds of Hz, the impact of f_s and L_1 on the proportionality between dissipation and resistance will be small, since the relative change in frequency is very small ($\sim 10^{-5}$) and since the change in L_1 is proportional to the change in frequency [9]. Consequently, when the changes in frequency are relatively small, the changes in dissipation will be directly proportional to changes in motional resistance. Therefore, dissipation and resistance can be treated as interchangeable entities under these conditions.

2.5 Sensing operation and decay length in a liquid

The reflection of the acoustic wave at the edges of TSM resonator is the basis for its oscillation. It is, however, the incompleteness of reflection that makes the device useful as a sensor. When a TSM resonator is immersed in a liquid, the quality factor drops drastically due to the acoustic coupling between the resonator and the liquid. This coupling is predominantly of a viscous character resulting in an increase in the motional resistance. The acoustic disturbance in the liquid, however, does not propagate since the shear modulus is zero and hence the acoustic wave will rapidly decay in the liquid. The decay of the wave can be described with the characteristic decay length, δ, which is the distance where the displacement amplitude has decreased to 1/e of its value at the surface. With η_l and ρ_l denoting the viscosity and density of the liquid, respectively, δ can be described [5]:

$$\delta = \left(\frac{\eta_l}{\pi f \rho_l}\right)^{1/2} \tag{2.5}$$

For a 10 MHz thickness shear resonator operating in water the characteristic decay length will be $\delta = 179$ nm. Figure 2.5 shows the normalized displacement in the liquid as a function of the distance from a 10 MHz TSM resonator immersed in water. The displacement of a resonator in a liquid, with half the viscosity of water, is shown for comparison. The decay in the lower viscosity liquid is notably faster.

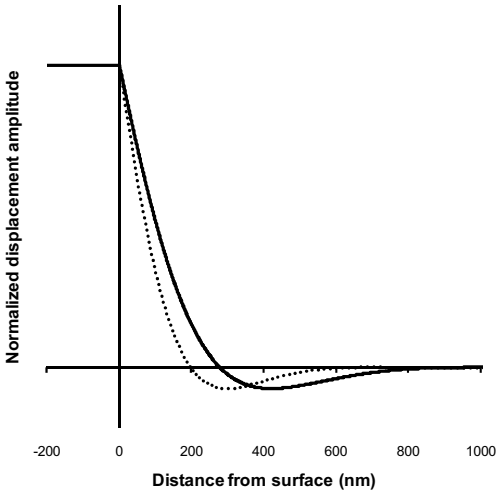

Figure 2.5. Displacement amplitude as a function of the distance from the surface of a TSM resonator immersed in a liquid. Solid line denotes resonator in water, whereas the dotted line represents the displacement in a liquid with half the viscosity of water.

With regards to sensor operation, the TSM resonator will be sensitive to any changes in the acoustic properties taking place within its decay function. Similar to optical biosensor techniques such as SPR, the response will vary with the distance from the surface. Different to optical sensors, however, is that binding of molecules to the surface may extend the decay length of the sensor if they provide an adlayer with higher viscosity than water, as discussed more in detail below.

2.6 Rigid, viscous and viscoelastic responses

To better understand thickness shear mode acoustics sensors, the sensor response to three different types of stimuli are considered and discussed; thin, purely rigid load, thick (thicker than the decay length) purely viscous load and viscoelastic loads of limited thicknesses respectively.

2.6.1 Rigid load

Thin rigid loads of the sensor are represented by a change in the inductance term in the equivalent circuit. The relationship between frequency and added mass can be described by the much cited Sauerbrey equation, which states that the frequency response is linearly proportional to the added mass [2]:

$$\Delta f = -\frac{2f_0^2}{\upsilon_q \rho_q}\frac{\Delta m}{A} \qquad 2.6$$

where f_0 is the resonance frequency, ρ_q the quartz density, υ_q the shear wave velocity in quartz and A the electrode area. The equation is valid if the added mass is much smaller than the mass of the crystal and that the added mass forms an evenly distributed rigid layer on the active sensor area. By addition of rigid loads to the sensor surface, the dissipation or resistance will remain unaffected. To illustrate this case of sensor perturbation, the displacement for a thickness shear mode resonator, operating in a liquid, with a thin, rigid film deposited on its surface is shown in Figure 2.6. The thickness of the film is represented by the dashed line, and as can be seen, the amplitude of the displacement is not affected within the film, but shows the same decay as for water outside the rigid film. The acoustic wave, in this case, can be considered to be extended to include also the added film, and thereby resulting in a frequency shift corresponding to the Sauerbrey equation.

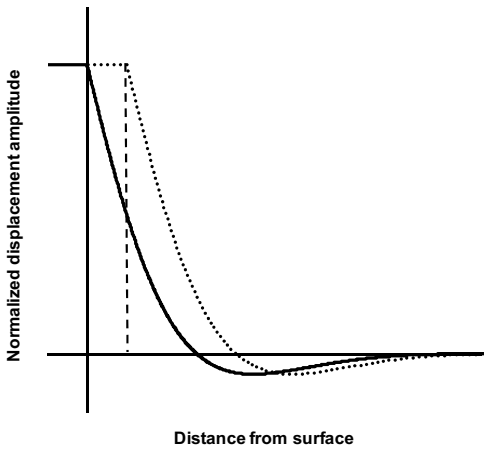

Figure 2.6. Amplitude displacement for a TSM resonator with a deposited, thin rigid film in liquid (dotted line). The film is indicated by the dashed line and the displacement for a resonator without the deposited film is shown for comparison.

2.6.2 Viscous load

Purely viscous loads of the sensor is represented in the equivalent circuit as a change in the resistance term due to viscous losses (damping) and changes in the inductance term due to coupled mass to the sensor surface by the viscous drag. The series resonance frequency and the dissipation (D_s) of an AT-cut quartz crystal have been found to be proportional to the square root of the density-viscosity product ($\rho_f\eta_f$) of a semi-infinite fluid in contact with the sensor surface according to the following expressions [9,13]:

$$\Delta f_s = \frac{\sqrt{f_s}}{2\sqrt{\pi} t_q \rho_q} \sqrt{\rho_f \eta_f} \qquad 2.7$$

$$\Delta D_s = \frac{1}{\sqrt{\pi f_s} t_q \rho_q} \sqrt{\rho_f \eta_f} \qquad 2.8$$

where ρ_q and t_q are the density and thickness of the quartz. The equations show that the frequency and the dissipation should be linearly dependent on each other when exposed to samples of varying viscosity and density as long as the change in frequency is relatively small. This has been experimentally shown with glucose-water mixtures and glycerol-water mixtures by Rodahl et al. [8] and Tsortos et al. [14], respectively. The displacement for different viscous loads on a TSM resonator is displayed in Figure 2.5 above.

2.6.3 Viscoelastic load and sensing of biomolecules

Turning to viscoelastic loads of limited thicknesses, most often encountered in studies of biomolecules, there is no simple equation that can predict the response of the resonance frequency and dissipation to biomolecular binding events. To assist the interpretation, a displacement profile for a TSM resonator with an arbitrary viscoelastic load is shown in Figure 2.7. The thickness of the viscoelastic layer is shown by the dashed line, wherein the variation in the displacement amplitude within the film is shown. Notably, the decrease in displacement amplitude is less than for the purely viscous load.

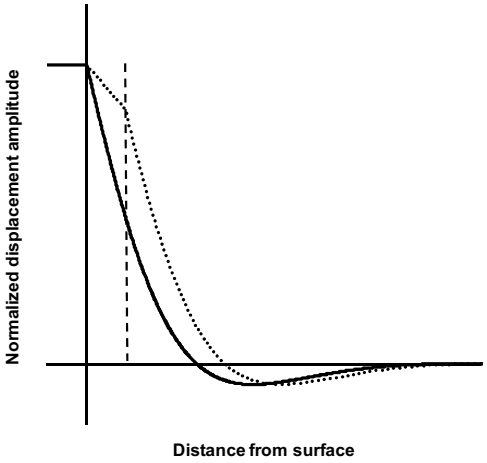

Figure 2.7. Displacement at TSM resonator by application of a viscoelastic load (dotted line). The thickness of the viscoelastic film is represented by a dashed line. Displacement decay in water is included as a reference.

With regards to biomolecule adsorption or binding to TSM resonator sensor surfaces varying degrees of viscoelasticity are likely to occur depending on the type of molecule and its mode of attachment to the surface. The response in resonance frequency is also likely to depend on the water coordination of a deposited film. For instance, DNA immobilization onto a QCM sensor surface has resulted in high dissipation responses, and frequency responses that leads to large overestimation of immobilized mass if the Sauerbrey equation is used [15,16]. Models have been developed to address the matter of viscoelastic adlayers [17,18]. These models predict that viscoelastic adlayers are underestimated in the frequency response, and by using overtones and dissipation data this can be accounted for. However, for studies of both protein and DNA adlayers these models provide estimates of bound mass that are even larger than the estimates from the Sauerbrey equation. Consequently, the concept of bound or hydrodynamically coupled water is often used to explain the disproportionate frequency responses. The following section will try to convey an understanding of this concept.

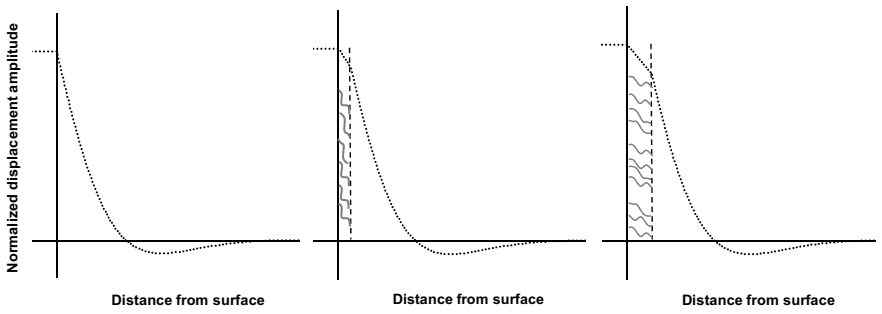

Figure 2.8 Displacement amplitude at the surface of a TSM resonator in liquid with only water (left), sparsely coated with DNA (middle) and densely coated with DNA (right). The thickness of the adlayers, denoted with a dashed line, is exaggerated in relation to the decay length for clarity of presentation.

Considering the case of DNA immobilization on the surface of a TSM resonator, Figure 2.8 illustrates schematically how the displacement amplitude may vary within the DNA layer and in the liquid. The thickness of the adlayers, denoted with a dashed line, is exaggerated in relation to the decay length for clarity of presentation. The left graph, representing a TSM resonator in water, is considered the starting point. When DNA molecules are added onto the surface, a layer with a thickness shown by the dashed line is formed on the surface, which results in the displacement amplitude changes shown in the middle graph. This means that the propagation of the wave is extended from the sensor surface and that the frequency response will depend on the acoustic properties within this whole region. In a simplified interpretation, the area under the curve is related to the frequency response; the larger the area, the larger the frequency response. The change in frequency will then be related to the change in area under the curve which in turn will depend on the thickness of adsorbed films. Consequently, the experienced frequency shift will not correspond only to the mass of the immobilized adlayer itself, but to the thickness that it spans beyond the surface and thereby also including the water that will be present within this layer. The thickness of the DNA film will likely depend on the chemical properties of the DNA and the density at which they are immobilized. Given the properties of DNA, which consist of charged strands compared to the more compact and complex structure of proteins, it seems likely that the thickness that DNA layers may span is greater than that of proteins with corresponding molecular weight. Thus, the higher degree of water coordination for DNA observed with QCM is likely due to its chemical structure.

An alternative approach to view water coordination on TSM resonators is to consider the coordinated water as being trapped and dragged along the sensor surface by the immobilized DNA strands. Referral to this phenome-

non as hydrodynamically coupled water then becomes more intuitive and comprehensive.

In summary, while the precise response of biomolecule binding to QCM sensor surface is difficult to describe due to molecular variations in water coordination and viscoelasticity, Muratsugu and coworkers showed by radioisotope labeling experiments that the linearity between the mass adsorbed and frequency response may persist under these conditions, but with a different coefficient for the frequency–mass relationship depending on the biological system [7]. The difference in the coefficients may then be explained by the varying degree of water coordination between different molecular species, which has been observed to correlate with the $\Delta R/\Delta f$ ratio of the binding event [11].

3 Molecular interaction studies

Biomolecules, such as nucleic acids, proteins and carbohydrates are important building blocks of living organisms. The different classes of biomolecules have different chemical structures appropriate for their biological tasks. For instance, sequences of deoxyribonucleic acid (DNA) are used for storage and transfer of genetic information. It consists of a linear chain of a saccaride-phosphate co-polymer, the backbone, to which nitrogenous bases are connected. The sequence of the four bases on the polymer constitutes the genetic code. The DNA structure is chemically stable, which is important for its purpose as genetic storage media. The stability and ability to conserve its code is further improved by base-pairing and formation of the well known double helix of the DNA made up from identical copies of single stranded DNA [19].

The genetic information of the DNA is translated, via ribonucleic acids (RNA), into proteins which are functionally involved in virtually every biological process. The tasks of proteins vary from enzymatic catalysis, for instance DNA replication, to muscular motion and immune protection. Proteins are all built from a set of 20 common amino acids that are linked together in a linear polymer, polypeptide, in a specific sequence that defines its function. In contrast to DNA, the proteins form complex three dimensional structures that are essential for fulfillment of their functional tasks. These structures can consist of several subunits that are linked together to form the complete macromolecule, which is the case for antibodies such as the depicted immunoglobulin G of Figure 3.1.

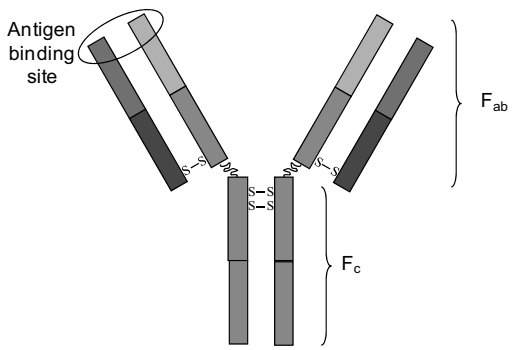

Figure 3.1. Schematic of immunoglobulin G structure.

The IgG structure is made up of the F_c (fragment crystallizable) region which is linked together with two identical F_{ab} (fragment antigen binding) regions. The F_{ab} fragments consist in a constant region and a variable region which is situated at the free end of the F_{ab} fragments. The variable regions form the paratope which can bind antigens with high specificity and affinity [20].

3.1 Protein interactions

Unlike covalent bonds between molecules, which involve the sharing of an electron pair between two atoms, association or binding between two proteins is the result of a multitude of weak bonds. These weak interactions are based on electrostatic, hydrophobic and van der Waals interactions, as well as hydrogen bonds, distributed over a binding surface that varies from 700 $Å^2$ to 4000$Å^2$. The binding enthalpies of these interactions are in the range of 2-13 kJ/mol, with van der Waals interactions in the lower end and hydrogen bonding in the higher, compared to 348 kJ/mol for a covalent carbon-carbon bond. While the interaction can consist of several ion pairs and hydrogen bonds and more than hundred van der Waals interactions, the aggregated bond strength will be higher. For instance, the strong binding of the bacterial protein barnase and its inhibitor barstar has a binding enthalpy of 80 kJ/mol [21,22].

3.2 Kinetics and affinity determination

Interactions between a two proteins that bind to each other with a one to one stoichiometry can be described by the equilibrium reaction

$$A + B \rightleftharpoons AB \tag{3.1}$$

This description of a interaction system is often referred to as a 1:1 interaction model or simple interaction model. The affinity of a molecular interaction is often given by its equilibrium dissociation constant, K_D, which is derived from the law of mass action according to

$$K_D = \frac{[A][B]}{[AB]} = \frac{k_{off}}{k_{on}} \tag{3.2}$$

The forward reaction rate or association rate, k_{on}, is the rate at which the complex AB is formed. The rate of AB dissociation is referred to as reverse reaction rate or dissociation rate, k_{off}. The affinity of an interaction can be determined by analysis at equilibrium, or by the ratio of the kinetic on and

off-rates as given by the equation above. In biosensor analysis, one of the binding partners, let say *B*, is immobilized on the surface typically by covalent attachment or by a biological interaction with a low off-rate such as by biotin-streptavidin capture. When the interacting partner, *A*, is flowed over the sensor surface, *A* will complex with the immobilized *B* and the response of the biosensor will be proportional to the concentration of the formed *AB* complex. In continuous flow biosensing, the time period when *A* is present over the sensor surface is often referred to as the association phase, whereas the dissociation phase is when the sensor flow cell has been purged with buffer and does not contain any significant concentration of *A*. To illustrate typical biosensor data, simulated sensor responses of two 50nM 1:1 interactions are shown in Figure 3.2. Sample concentrations based on a threefold dilution series ranging from 10 nM to 810 nM was simulated with an association phase of 100 s, and a maximum binding capacity, B_{tot}, of 100 (arbitrary units). The data sets are different in that the left set (a) shows data with ten times faster association and dissociation rates than the right data set (b). This shows how different the binding characteristics can be for interactions with equal affinities and emphasizes the necessity of obtaining the kinetic rate parameters of a studied interaction pair.

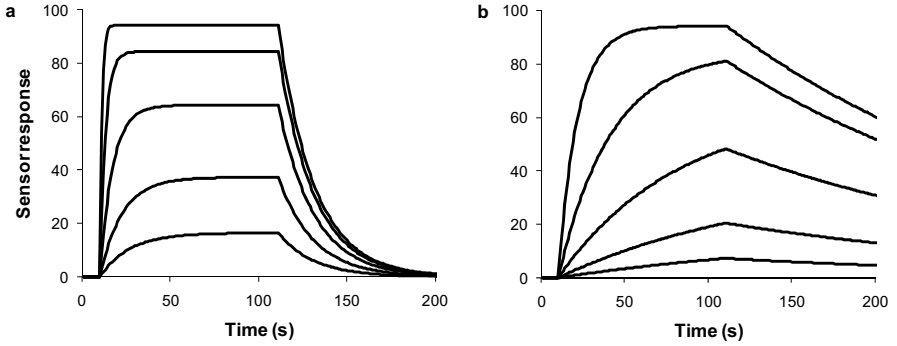

Figure 3.2 Simulated biosensor data for two 1:1 interactions with 50 nM affinity, with concentrations ranging from 10 nM to 810 nM in three fold increments. Data set (a) shows the interaction with an on-rate of 1×10^{6} $M^{-1}s^{-1}$ and off-rate of 5×10^{-2} s^{-1}.The corresponding on-rate for the data set (b) was 1×10^{5} $M^{-1}s^{-1}$ and the off-rate of 5×10^{-3} s^{-1}.

Kinetic rates for biological systems can vary significantly. Association rates can be found in the range of 10^{3} to 10^{9} $M^{-1}s^{-1}$, although most known interactions have association rates of 10^{5} to 10^{6} $M^{-1}s^{-1}$. Measured rates of dissociation are found in the range of 10^{0}-10^{-5} s^{-1}, although slower dissociation rates exist but are more challenging to accurately measure [21]. As an example of a biological system with very fast on-rate, the interaction between barnase and barstar mentioned above has an on-rate of 4×10^{8} $M^{-1}s^{-1}$ and an off-rate of 4×10^{-6} s^{-1}. The affinity of $K_D = 1\times10^{-14}$ M, as a result of an extremely fast on-

rate and a very slow off-rate, is very high and is only superseded by very few interaction pairs, such as the biotin-avidin interaction that has an affinity determined to 6×10^{-16} M [23].

As mentioned above, the affinity of an interaction can be determined using equilibrium data such as the data set of Figure 3.2a. In this data set, equilibrium has been reached as evident from the plateaus in the sensor response which indicate that here the forward rate is equal to the reverse rate of *AB* complex formation. The basic relationships that are applied to determine affinity at steady state are briefly described in the following section. First, the change of *AB* concentration with time can be expressed as

$$\frac{d[AB]}{dt} = k_{on}[A][B] - k_{off}[AB] \tag{3.3}$$

With the total concentration of immobilized receptors expressed in terms of free and bound concentrations

$$[B]_{tot} = [B] + [AB] \tag{3.4}$$

The rate of *AB* conversion can be written as

$$\frac{d[AB]}{dt} = k_{on}[A]([B]_{tot} - [AB]) - k_{off}[AB] \tag{3.5}$$

At steady state, equilibrium, the change in *AB* concentration is zero and equation 3.5 can be transformed into

$$[AB] = -K_D \frac{[AB]}{[A]} + [B]_{tot} \tag{3.6}$$

Expression 3.6 has the form of a straight line. By plotting the frequency response at equilibrium as function of the frequency response over the respective concentration of *A* the equilibrium dissociation can be determine as the magnitude of the line slope, and the response maximum corresponding to the total concentration of immobilized receptors as the line's intercept with the y-axis. The method is illustrated in Figure 3.3, where equilibrium data from previously shown simulations (Figure 3.2a), were recovered and plotted.

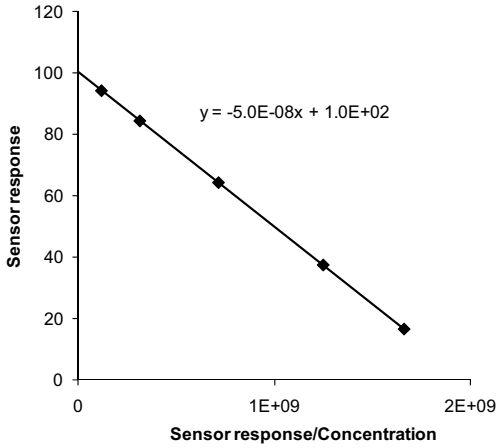

Figure 3.3 Determination of equilibrium dissociation constant at steady state by means of a Scatchard plot. The determined K_D and B_{tot} were consistent with simulation data input as indicated by the equation inset.

Determination of kinetic rate constants from biosensor interaction data can be done by several different methods, such as linearization and numerical integration [24]. To use the linearization approach, equation 3.5 is rewritten by substituting *[AB]* with the response, *R,* since the sensor response will be proportional to the complex concentration. Also, $[B]_{tot}$ is replaced with theoretical response maximum, R_{max}, which is proportional to $[B]_{tot}$

$$\frac{dR}{dt} = k_{on}[A][R]_{max} - R(k_{on}[A]+k_{off}) \qquad 3.7$$

By plotting *dR/dt* versus *R* the slopes of the curves will correspond to $-(k_{on}[A]+k_{off})$, which is in turn plotted over the respective concentrations to yield k_{on} as the slope of this line. During the dissociation phase the concentration of *A* is zero and therefore equation 3.7 becomes

$$\frac{dR}{dt} = -k_{off}R \qquad 3.8$$

By integration of equation 3.8 the sensor response can be expressed

$$R = R_0 e^{-k_{off}t} \qquad 3.9$$

To determine the off-rate, $ln(R_0/R)$ is plotted over time to provide the k_{off} as the slope of the line. The linearization procedure for determination of kinetic rates was carried out on the dataset of Figure 3.2b and is displayed in Figure 3.4 below. Notably, despite conducting the analysis on perfect simulated data, a 5% error is seen in the determined on-rate.

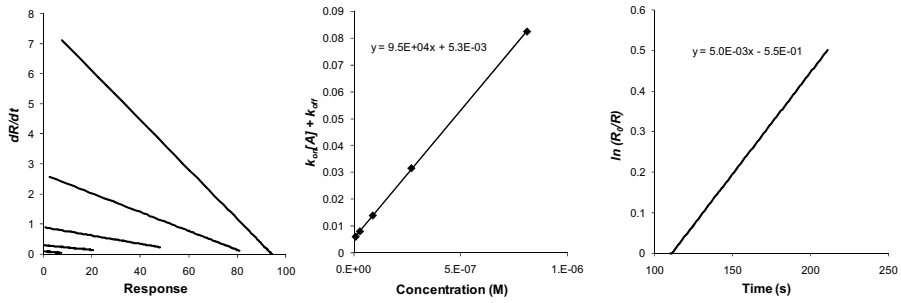

Figure 3.4 Linearization procedure for determination of kinetic on and off-rates.

As an alternative to the shown linearization procedure, the fitting of sensor data to the integrated rate equation is possible. The integrated rate equation based on equation 3.7 provides the following expression for the sensor response as function of time and concentration of *A*

$$R = \frac{[A]k_{on}R_{max}}{[A]k_{on}+k_{off}}\left(1 - e^{-([A]k_{on}+k_{off})t}\right) \qquad 3.10$$

The most robust method for determining kinetic reaction rates, however, has been shown to be numerical integration of the rate equation and fitting to experimental data by error minimization algorithms. In particular, global data fits on complete sets of data with analytes injected at several different concentrations and simultaneously fitting association and dissociation phases has been proved successful, also for more complex interaction models [24,25].

3.3 Sample introduction and mass transport

A prerequisite for the described kinetic and affinity analyses is that the concentration of the analyte over the surface needs to be known. In a continuous flow biosensor system, such as the one displayed in Figure 3.5, running buffer is continuously flown over the sensor surface at a given flow rate. To introduce sample over the sensor, the injection loop is filled with sample, which is then entered into the flow line by switching of the injection valve. The sample is thereby transported to the sensor surface by continuously flowing running buffer.

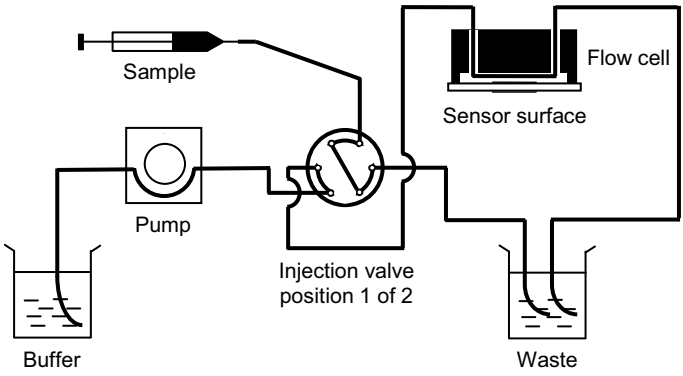

Figure 3.5 Schematic of a continuous flow biosensor system describing the flow path for running buffer and sample.

The flow conditions in micro analytical sensor systems will be of laminar nature due to the small dimensions typically used in these systems. In laminar flow, a parabolic profile of the flow velocity in the flow lines and flow cell is given. The flow velocity will be the fastest in the middle of the flow channel, and will decrease towards the edges to become essentially stagnant at the channel walls. In biosensing, this has two important implications; first the sample that is injected into the loop of the injection valve and later flown into the flow cell will be affected by this flow velocity profile. Together with radial diffusion in the flow line this will result in dispersion of the sample plug. The dispersion of the sample plug results in a concentration gradient in the beginning and end of the plug, during which the precise analyte concentration over the sensor surface is difficult to predict. The extent of dispersion is dependent on the dimensions of the flow channel, and to reduce impact of dispersion the distances and volumes between injection valve and flow cell should be kept short. A typical appearance of a sample plug from an Attana A100 QCM biosensor system is shown in Figure 3.6 for a set of glycerol samples with concentrations ranging from 0.25 to 5% of glycerol in water.

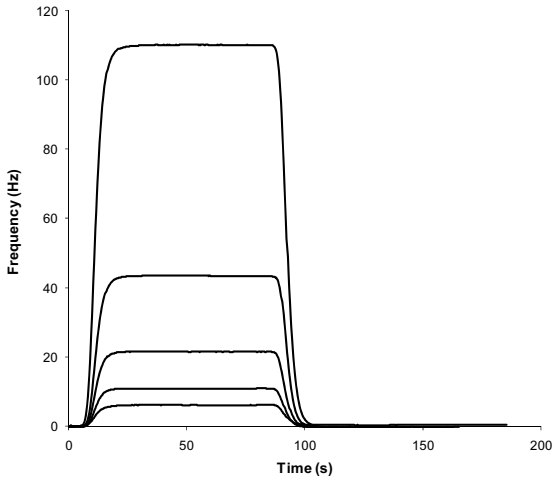

Figure 3.6 Real-time frequency data for a series of glycerol concentrations ranging from 0.25 to 5% (w/v) in water. For consistence with other biosensor techniques and clarity in view, the inversed frequency shift is presented.

The glycerol samples reach the sensor approximately 10 seconds after the sample has been introduced in the flow by the injection valve. When the sample reaches the sensor, the change in viscous load results in a signal increase with a rise time, typically around 10 s before the sensor reaches a stable value. This rise phase of the presented data is considered mainly to be the result of dispersion in the flow channel between the injection valve and the sensor as well as dispersion within the sensor flow cell itself. In the context of rate constants determination, the concentration gradients observed in the beginning and end of the injection can be managed by excluding these sections from the data analysis. Except for interaction systems that equilibrate very rapidly due to fast off-rates, this data exclusion will not limit the ability to determine the kinetic rate constants.

The second impact of the parabolic flow is that the flow rate close to the sensor surface will be very slow, and that molecular transportation in this domain relies on diffusion. Figure 3.7 shows a schematic of the flow conditions over a biosensor surface with a stagnant zone of arbitrary thickness, b. As the sample enters over the sensor surface, free analyte will diffuse to the immobilized interaction partner and bind with it. If the diffusion to the surface is significantly faster than the binding reaction, the concentration of analyte at the surface will be essentially the same as in the bulk of the liquid. On the other hand, if the diffusion rate is similar or slower than the reaction rate, the analyte at the surface will be depleted by the binding reaction and the concentration at the surface will be different than in bulk liquid. When the concentration close to the surface is not known, the methods to determine kinetic rates previously described herein cannot be applied.

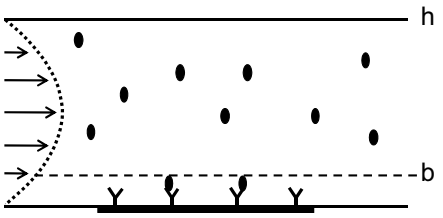

Figure 3.7 Schematic picture illustrating the flow conditions close to a biosensor surface. Flow cell height is denoted by h whereas b denotes stagnant zone over the sensor surface.

To address this, however, several measures can be taken. The flow velocity over the surface can be increased by running the experiments at higher flow rate, or by lowering the flow cell dimensions. This will improve diffusive flow to the surface since the height of the stagnant zone will decrease. Also, the density of immobilized receptors can be reduced, if the sensitivity of the assay allows it. This will reduce the reaction induced analyte depletion at the surface. Alternatively, or in addition to experimental modifications, the interaction model for data evaluation can be amended. By introducing a model of the flow cell and sensor surface which has two compartments, one with the bulk concentration of analyte and one which is dependent on diffusion of analyte from the bulk and the reactions on the surface [25]. With the bulk concentration defined as A_0 the following reaction is defined, with the transport coefficient, k_M, as both forward and reverse rate.

$$A_0 \rightleftharpoons A \qquad 3.11$$

This modification of the previously described 1:1 interaction model results in an equation system of two interdependent differential equations. The methods of numerical integration mentioned previously can be applied to extract the reaction rates for the interaction, together with the transport coefficient. To illustrate the impact of diffusion limitations to biosensor data, the fast 50 nM interaction used above was modeled with mass transport limitations as shown in Figure 3.8a. The unperturbed data set is included for comparison. The ability to resolve correct kinetic rates for the interaction was demonstrated in Figure 3.8b by subjecting the data set to global curve fitting by numerical integration in the CLAMP software developed by Morton and Myszka [26]. The on and off-rates obtained by curve fitting were found to be in good agreement with the data that was used to create the data sets by simulations.

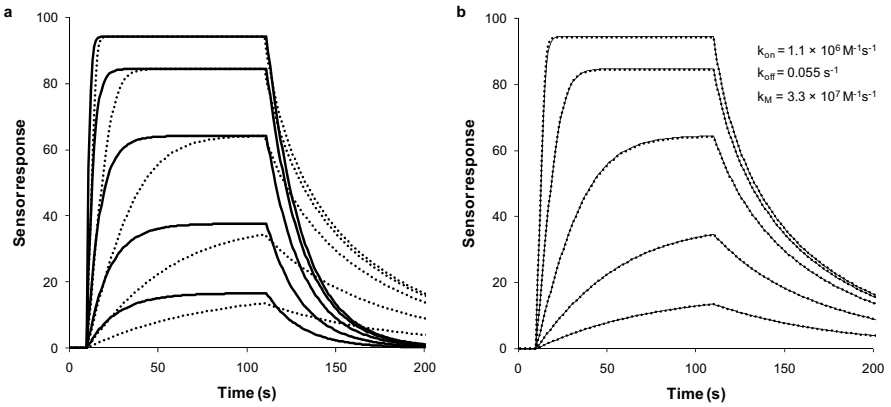

Figure 3.8. a) Simulated data for a 50 nM interaction with (dotted line) and without (solid line) mass transport limitations. b) Simulated interaction data of mass transport limited data (dotted line) together with global data fit (thin solid line) according to the two compartment model in CLAMP. The simulation conducted with an on-rate of 1×10^6 $M^{-1}s^{-1}$ and an off rate of 5×10^{-2} s^{-1} to be compared with the data from the curve fitting shown in the inset.

4 Biosensor assays (Paper I)

Real-time biosensors can be used in different ways to obtain information regarding biomolecular interactions. Kinetic and equilibrium assays, as described in the previous section are only two possibilities. Competition or inhibition assays can also be employed on biosensors to provide the desired biological data. In a competition assay the affinity of an interaction is assessed indirectly by allowing the examined ligand to compete with the interaction of a known reference ligand to an interacting receptor. The concentration of the studied ligand is varied, whereas the concentrations of the reference ligand and interacting receptor are kept constant. The response of reference ligand-receptor binding is plotted against the competitor concentration. At the concentration which results in half the maximum binding the effective concentration, EC_{50}, is defined. EC_{50} values are closely related to the affinity dissociation constant and are frequently used for affinity ranking of different ligands within biological research and pharmaceutical development.

In Paper I, a competitive assay for quantitative analyses of carbohydrate-lectin interactions was developed on a novel continuous flow QCM biosensor. Lectins are carbohydrate binding proteins, and the plant lectin concanavalin A (Con A) is well known to interact with yeast mannan, a mannose-rich polysaccharide. The developed method relies on immobilization of yeast mannan on the QCM sensor, and subsequent measurement of the binding of Con A to the surface under competing conditions. The method proved to be highly functional, and the obtained data was found to be in good agreement with previously published data from enzyme-linked lectin assays (ELLA). The advantage over the previously known methods was that the interactions were monitored in real-time without the need for reagent labeling.

As several of the steps of the development of this assay are generally applicable for development of biosensor assays, they will be discussed in more detail. In the development of the assay, the first step was immobilization of the mannan on the sensor surface. For the initial tests, a straightforward approach for adsorption of the mannan on gold surfaces was chosen. However, since adsorption to gold was unsuccessful, QCM surfaces were coated with polystyrene to mimic conditions used in the ELLA format. The coated crystals were inserted into the QCM flow-through system and were subjected to repetitive injections of mannan to obtain a saturated surface as shown in Figure 4.1a. To avoid non-specific binding to remaining uncoated hydrophobic regions of the sensor surface, bovine serum albumin (BSA) was in-

jected repeatedly over the surface until no more binding was observed. The binding capacity of the sensor surface was subsequently tested by injections of Con A as shown in Figure 4.1b. The Con A response was around 110 Hz, which was considered satisfactory based on the resolution requirements of the assay and the instrumentation noise level.

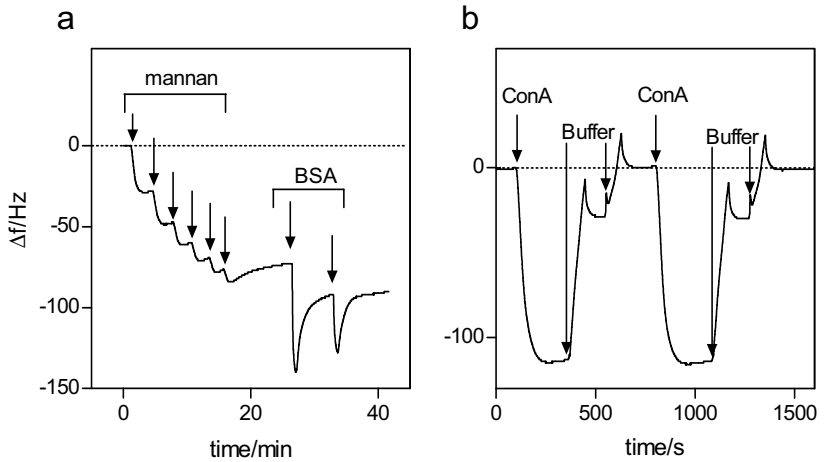

Figure 4.1.a) Immobilization of yeast mannan and subsequent blocking with BSA of a polystyrene QCM sensor surface. b) Repetitive binding of Con A to the mannan surface with intermediate regeneration by duplicate injection of acidified PBS buffer. Negative frequency changes correspond to binding to the sensor surface.

A second step in the assay development was to establish suitable regeneration conditions for removing the bound Con A from the mannan surface. Finding good regeneration conditions is often an iterative procedure that may sometimes be very time consuming. Typically used regeneration conditions with respect to the immobilized species are acids (5-150mM) for antibodies and proteins, SDS (0.01-0.5%) for peptides and nucleic acids, and sodium hydroxide (10mM) for hybridized nucleic acids [27]. Contact times and concentrations can be varied and also combinations and sequences of injections may be necessary to reach the desired result. For the interaction between mannan and Con A, two methods were evaluated; competition with excess of carbohydrate ligands and injections of acidified PBS. Injection of competing ligands proved feasible, but required multiple pulses before the original baseline could be restored making the method less time efficient. Duplicate injections of acidified PBS buffer at pH 1.5, however, proved effective in removing the bound Con A, and restored the baseline to the original level as shown in Figure 4.1b. Also, the close to identical Con A binding levels achieved before and after regeneration proves that the regeneration conditions were indeed successful in removing all bound Con A and that the surface with immobilized mannan was not degenerated by the chosen set of conditions.

A third important step in preparation of the assay is to ensure that the registered signal is actually due to the interaction of interest and not due to non-specific binding. This can be tested by running the samples also over a reference surface with similar properties as the interaction surface, but without the interaction partner itself. This method is normally convenient if the sensor system is equipped with two or more channels, but is always subject to the difficulty of finding the optimal reference surface. Non-specific binding can also be tested by injection of an irrelevant protein over the sensor surface that is known not to interact with the immobilized ligand. In this study, this was tested subjecting the mannan surface to injections of mistletoe lectin, which specifically binds to other carbohydrates than those of the mannan polysaccharide. The mistletoe lectin resulted in very small frequency responses, which indicated that the interaction seen for Con A was indeed biospecific. As an additional test of the specificity of the assay, Con A was injected together with a competitor ligand and a ligand without known interaction to the relevant binding site. In this test the competitor significantly reduced the binding of Con A to the surface, whereas the inactive ligand had no effect on Con A binding, further proving the specificity of the assay. Finally, it should be mentioned that competition assays such as this one is not very sensitive to moderate amounts of non-specific binding as given by the evaluation procedure below.

The fourth step in the development of this assay was to certify that equilibrium was reached for the chosen experimental conditions. This step is not necessary for kinetic assays, but equilibrium based analysis such as competition assays require steady state to be reached during the association phase as described in the previous section. To assess whether equilibrium is reached, the real-time interaction data can be examined. If a stable response level is reached during the association phase, this indicates that equilibrium has been reached. Alternatively, the apparent equilibrium binding data can be put into a Scatchard plot and the linearity of the curve will indicate if equilibrium has been reached. A similar test, but possibly more robust to data errors, is to fit the binding data by non-linear regression to the Langmuir isotherm. This was done for the presented study, and the Con A to mannan binding data was shown to adhere well to Langmuir-like adsorption characteristics, as indicative of equilibrium binding data.

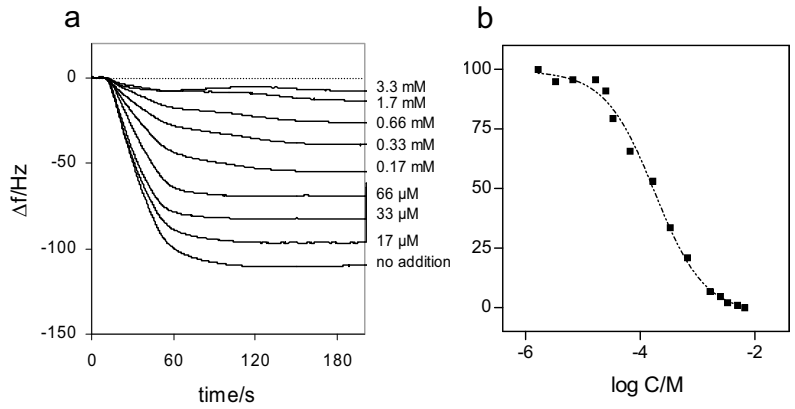

Figure 4.2. a) Frequency response plots of the inhibitory effect of PNP-mannose on Con A/mannan binding. Increasing concentrations of competitor resulted in reduced frequency response. b) Competition plot for PNP-mannose and a curve fit that provides an EC_{50} of 0.18mM for PNP-mannose.

After the four steps of assay preparation and validation, the assay was used to assess the competitive effect of the carbohydrate PNP-mannose to the Con A – mannan binding as shown in Figure 4.2a for a set of concentrations of PNP-mannose together with Con A. The competitive effect is clearly seen as the decrease in Con A binding to the mannan surface. To determine the EC50 value, the competition data was transformed into relative binding data and plotted against the logarithmic concentration as shown in Figure 4.2b. The data was fitted by non-linear regression to determine the EC 50 value according to the following equation:

$$\Delta f = \Delta f_{min} + \left(\frac{\Delta f_{max} - \Delta f_{min}}{1+10^{(C-logEC_{50})}}\right) \qquad 4.1$$

The fitted maximum response without the presence of the competitor is denoted Δf_{max} and Δf_{min} is the fitted minimum response for the highest concentration of competitor. As given by the equation, Δf_{min} is subtracted from the data, thereby removing potential bias from non-specific binding in the analysis. As mentioned above, the data derived by this method for the PNP-mannose and three other carbohydrates were found to be in good correlation with previously reported data. In summary, this section has described the development of a competition biosensor assay. By doing this, four steps that is generic for many biosensor assays have been presented and discussed. Establishing a reliable immobilization method, suitable regeneration conditions and checking data for contribution from non-specific binding are steps that always need to be fulfilled for successful biosensor studies. In addition, for steady-state equilibrium assays it is important that true equilibrium conditions are verified, whereas kinetic assays require that the impact of mass transport limitations is investigated and controlled to acceptable levels.

5 Surfaces and immobilization (Paper II-IV)

For successful interaction studies with biosensor instrumentation, one binding partner needs to be immobilized on the surface. The immobilization method should be reproducible, versatile and easy to use. Furthermore, it is important to obtain sufficient density of the immobilized molecule on the surface where the molecule should retain biological activity in its immobilized state and withstand regeneration conditions used to remove interacting analytes. While proteins and other biomolecules are a very diverse group of molecules, significant challenges exist in order to develop methods that fulfill all of the requirements above, for all possible molecules that one would like to immobilize.

Three different studies of surfaces and immobilization methods have been conducted. In Paper II preparation conditions for sensor surfaces based on carboxyl-terminated self assembled monolayers were optimised. Paper III evaluates a method for immobilization of very acidic biomolecules based on the use of an electric field. Finally, in Paper IV a method for immobilization on a carboxyl surface was optimised and the influence of immoblisation pH on the immobilization response and antigen binding capacity was thoroughly assessed.

5.1 SAMs and OEG-SAM chemistry (Paper II)

Self-assembled monolayers (SAMs) prepared from alkylthiols on gold are commonly used as highly robust coating materials in biosensor development. Different chemical and biological functionalities can easily be incorporated to tailor the SAM surface properties [28,29]. For preparation of SAMs based on alkylthiols, a clean gold substrate is immersed in a micro to milli-molar concentration of the thiol in ethanol as shown by the schematic in Figure 5.3. Initial adsorption of thiols to the gold surface is fast, whereas the ordering of the alkyl chains to an almost crystalline structure takes hours to days [28,30]. The preparation conditions are of great importance in order to achieve high quality SAMs. Factors that may influence the rate of adsorption as well as the structure of the SAM include choice of solvent, temperature, concentration, molecular structure of the thiol, immersion time and purity of the substrate [28].

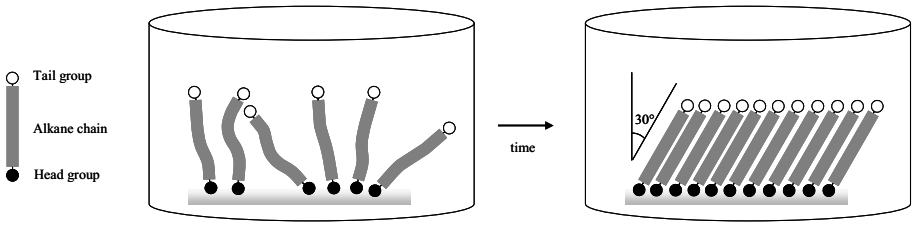

Figure 5.1. Schematic picture describing the formation of a SAM from a diluted alkyl-thiol solution. The initial unordered SAM transforms to a dense and well-ordered SAM with incubation time.

Sensor surfaces to be used for immobilization of biomolecules require presence of functional groups that are accessible on the surface. For instance, carboxyl groups are frequently used for immobilization of biomolecules on carboxy-methylated dextran (CM dextran) surfaces by means of the amine coupling procedure [31,32]. Carboxyl groups can readily be incorporated in SAMs, but optimal preparation methods have previously not been satisfactorily established. Carboxylic acid terminated SAMs have been reported to form unstructured SAMs due to repulsion between the charged carboxylate groups. As a means of getting well-ordered carboxyl SAMs it has thus been suggested that the thiol solution should be acidified [33,34]. The effect of the addition of acid in the thiol solution has been studied in Paper II and was shown to improve the organization within the SAMs. However, it was demonstrated that the carboxyl acid groups were rapidly converted to an ethyl ester in the presence of hydrochloric acid (HCl), which reduces the functionality of the surface for biosensing since the formed esters are inert to the amine coupling procedure. Alternatively, an improved SAM structure was shown achievable by a weaker acid such as acetic acid (HAc), but also this procedure resulted in esterification albeit at a much slower rate. The esterification process is illustrated in Figure 5.2, where the formation of the ethyl ester in the presence of HCl and HAc is shown as a function of solution age/incubation time. The rate of esterification was strongly dependent on the strength of the acid.

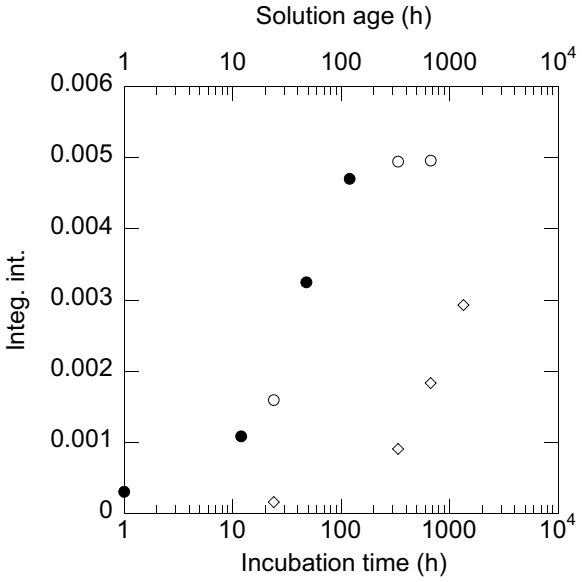

Figure 5.2. Integrated intensities of the CH_3 peak in infrared adsorption spectra from the HCl and HAc SAM surfaces representing the progress of esterification. The filled symbols, ● HCl, belong to the lower x-axis and refer to experiments with varied incubation time. The open symbols, ○ HCl and ◊ HAc, belong to the upper x-axis and refer to experiments where the age of the incubation solution has been varied.

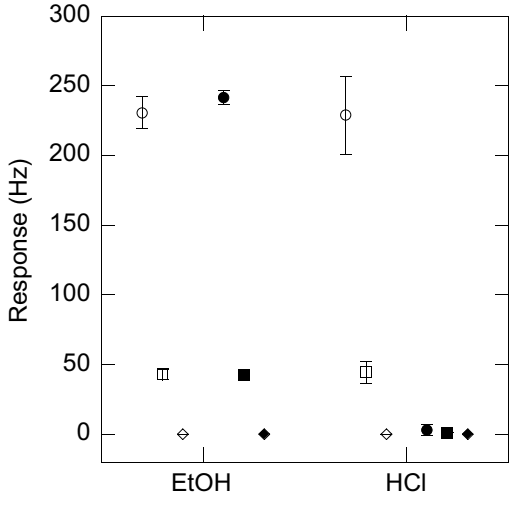

Figure 5.3. QCM data of OEG-COOH SAMs formed from fresh and 4 weeks old thiol solutions. ○ anti-myoglobin 7005 immobilization fresh solution, ● anti-myoglobin 7005 immobilization 4 weeks old solution, □ myoglobin binding fresh solution, ■ myoglobin binding 4 weeks old solution, ◊ myoglobin non-specific binding fresh solution and ♦ myoglobin non-specific binding 4 weeks old solution.

Functional evaluation of sensor surfaces prepared both in absence and presence of acid was conducted by immobilization of an antibody on these surfaces and by monitoring the interaction with its antigen in QCM. This evaluation revealed that the surfaces were highly functional as biosensor surfaces with both reproducible antibody immobilization and interaction with its antigen as shown in Figure 5.3. The impact of acid treatment on one day old solutions showed that the antibody-antigen system studied was surprisingly insensitive to the degree of esterification of the carboxylic acid SAMs. However, 4 weeks of storage of the two investigated thiols in hydrochloric acid containing ethanol resulted in SAMs that were completely inactive with respect to immobilization and subsequent binding of the antigen. Non-specific binding to the surfaces was also studied and it was encouraging to note that the non-specific binding of both antigen and antibody was extremely low on the two SAMs, regardless of the relative amount of ethyl esters on the surface.

5.2 Electric field assisted immobilization (Paper III)

Immobilization of certain biomolecules on sensor surfaces may be more challenging than others. For instance, the proinsulin C-peptide has a very low pI (pI 3.3), which prohibits immobilization on a carboxyl surface by conventional amine coupling methods. To address this, a method was developed to facilitate immobilization of very acidic molecules by applying an external electric field over the sensor surface and flow cell (Paper III).

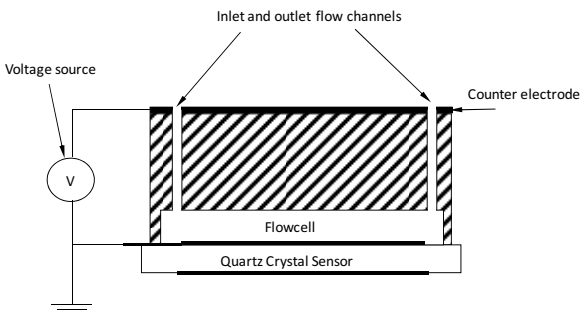

Figure 5.4. Schematic illustration of flow cell and connections to voltage source.

The biosensor flow cell was modified by connecting the sensor electrode of the quartz crystal and a counter electrode positioned on the flow cell to a voltage source as shown in Figure 5.4. By applying different potentials over these electrodes, an electric field over the flow cell could be controlled.

Amine coupling onto a carboxyl sensor surface involves first activation of the sensor surface with a 1-ethyl-3-[3-dimethylaminopropyl] carbodiimide hydrochloride (EDC) and N-hydroxy-succinimide (NHS) reagent mixture.

This process transforms carboxyl groups on the surface to active esters that are relatively stable, and yet good leaving groups. In the second step, the protein is introduced over the surface and its primary amine groups will bind to the carbonyl group of the activated esters. For the binding of the protein to occur, the protein needs to be transported to the sensor surface. Electrostatic attraction between the sensor surface and the protein is necessary to achieve this at acceptable protein concentrations, and consequently the protein is introduced over the sensor surface in a low ionic strength buffer at a pH lower than its pI [31]. Under these conditions, the protein overall charge is positive, whereas the sensor surface carboxyl groups present a negative charge thereby providing the necessary electrostatic attraction. The charge on the sensor surface is, however, dependent on the surface acid dissociation constant (pKa). If the pH of the immobilization buffer is significantly below this pKa, then the surface will be essentially charge neutral whereby the attraction to the surface and consequently immobilization will be ineffective. The low pI of the C-peptide means that the immobilization buffer needs to be at pH 3 or lower to make the peptide positively charged. At this pH both CM dextran (pKa ~3.8) and carboxyl SAM (pKa ~5) based sensor surfaces will be essentially non-charged [35].

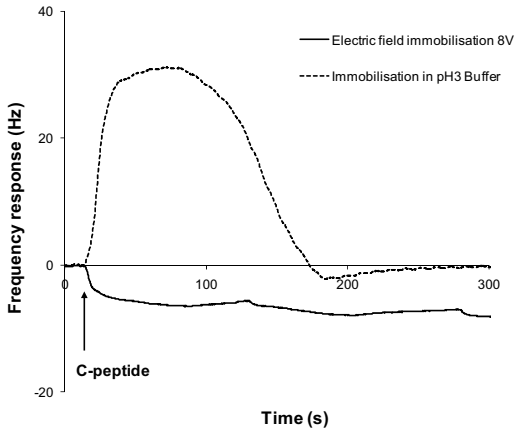

Figure 5.5. Electric field assisted immobilization of C-peptide on a SAM carboxyl sensor surface (solid line). Immobilization attempt with C-peptide in pH 3 immobilization buffer is shown as comparison (dashed line).

Immobilization attempts on EDC/NHS activated carboxyl sensor surfaces with and without an externally applied electric field with the C-peptide injected under neutral or acidic (pH 3) conditions, respectively, are shown in Figure 5.5. Approximately 10 Hz of the C-peptide was bound to the sensor surface when an electric field was applied to facilitate the transport to the sensor surface. Presence of C-peptide on the sensor surface was confirmed by injections of a C-peptide specific monoclonal antibody. Comparative data

for the immobilization attempt at pH 3 shows a reversible buffer response during the injection but no remaining frequency shift representing C-peptide immobilization. The approach to use an externally applied electric field to immobilize acidic peptides on carboxylated sensor surfaces was thereby proven successful.

5.3 Antibody immobilization (Paper IV)

Protein and peptide immobilization on SAM-based sensor surfaces has been demonstrated in the previous section, but a detailed examination of the performance of SAM carboxyl surfaces is still justified. Paper IV describes the optimization of immobilization conditions for antibodies on two dimensional carboxyl sensor surfaces, and the impact of antibody orientation on the antigen binding capacity.

The ability to attach a protein to a biosensor surface is highly dependent on the electrostatic attraction to the sensor surface as discussed above. While polymeric sensor surfaces such as the CM dextran is capable of providing an almost unlimited amount of a carboxyl groups, a two dimensional surface can only hold a confined number of carboxyl groups that can be activated. By the activation, these carboxyl groups can be substituted completely, or to a high degree, by neutral NHS groups leading to loss of attractive charges on the sensor surface. In addition, the relatively high surface pKa of SAM carboxyl sensor surfaces limits immobilization with standard EDC/NHS activation reagents to relatively high pH. Therefore, the neutrally charged NHS was substituted with N-hydroxysulfo-succinimide (sulfo-NHS). Sulfo-NHS has a very low pK_a and exchanging NHS for the sulfo-substituted analogue should provide an activation method that ensures that the surface is negatively charged at all relevant pHs. To illustrate the effect of different activation reagents on surface charges, a schematic of carboxyl surfaces activated with EDC, EDC/NHS and EDC/sulfo-NHS is shown in Figure 5.6.

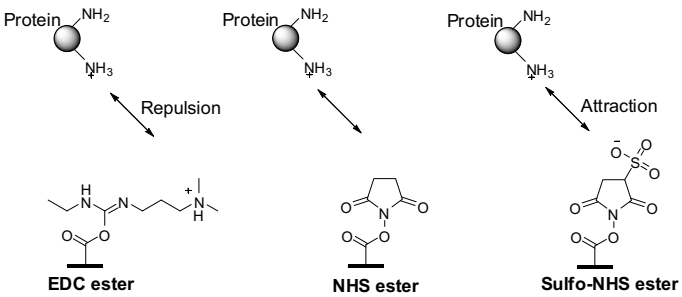

Figure 5.6. The dissimilar modification to the surface charge that is the result of activation with EDC, EDC/NHS or EDC/sulfo-NHS, respectively.

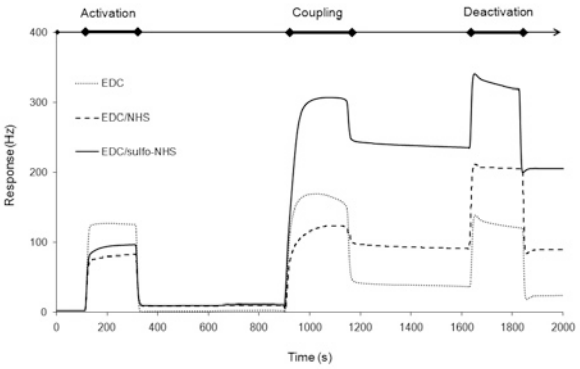

Figure 5.7. Monoclonal antibody immobilized on a carboxyl surface activated by EDC (dotted line), EDC/NHS (dashed line), and EDC/sulfo-NHS (solid line), respectively

In order to study the effect of activation reagents systematically, carboxyl surfaces were activated by EDC, EDC/NHS or EDC/sulfo-NHS reagent mixtures, respectively, and a monoclonal antibody in pH 4.5 of acetate buffer were subsequently injected. The results are shown in Figure 5.7, which clearly demonstrate that the most efficient immobilization was obtained on carboxyl surfaces activated by EDC/sulfo-NHS, whereas less efficient coupling responses are achieved with surfaces activated by EDC or EDC/ NHS. The higher immobilization level of EDC/sulfo-NHS activated surface compared to the EDC/NHS activated surface is believed to be due to the retention of negative surface charge throughout the activation and coupling process. The improvement in surface charge is due to a two-fold mechanism; for each carboxyl group activated with NHS, one surface charge is removed, whereas the negative charge will be retained with sulfo-NHS. Secondly, the potentially remaining carboxyl groups will lose their charges as pH decreases, whereas the charge of the sulfo group is unaffected by the pH changes. The low immobilization response of the EDC activated surface can be explained by a similar argument, but more accentuated, since the EDC ester will be positively charged. These results show that electrostatic attraction is essential for successful immobilization on two-dimensional carboxyl surfaces and the use of the EDC/sulfo-NHS reagent mixture provides an effective method to accomplish this.

For an immobilization method to be useful for biosensor purposes, the immobilized proteins need to remain biologically active on the surface. To examine the pH dependence on antibody immobilization levels and antigen binding capacity, four different antibodies were immobilized on SAM carboxyl surfaces with the EDC/sulfo-NHS reagent mixture. A high pI of the antibody enabled immobilization over a wide pH range, whereas a low pI limited immobilization to low pH, as could be expected. The antigen binding capacity followed the immobilization response in most cases. However, the

antigen to antibody binding ratio differed between the antibodies investigated, and for one of the antibodies, the antigen binding capacity was significantly lower than expected from the immobilization level in a certain pH range. To examine the impact of antibody orientation on the binding capacity, the ratio between antigen binding (AG) and antibody immobilization (AB) responses were plotted over the tested pH range as shown in Figure 5.8. If the orientation is assumed to be the predominant cause of variations in AG to AB ratios, while disregarding small differences in molecular weight between the antigens, a high AG to AB ratio should indicate an orientation of the antibody with the Fab portions exposed. Conversely, a low AG to AB ratio should imply more hidden Fab portions and exposed Fc portions. To test this hypothesis, surfaces with high and low AG to AB ratios were tested for binding of Fc and Fab specific antibodies. These tests confirmed that the orientation of the antibodies on the surface had a profound effect on the antigen binding capacity of the immobilized antibodies.

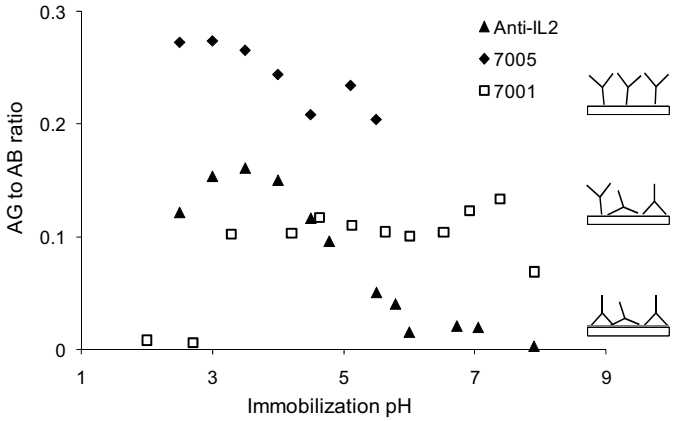

Figure 5.8. Antigen (AG) to antibody (AB) response ratios of anti-myoglobin 7005 (filled diamonds), anti-myoglobin 7001 (open squares) and anti-interleukin 2 (filled triangles) over the immobilization pH. The scheme to the right illustrates a potential interpretation of the variation in AG to AB ratios by showing antibodies immobilized on a sensor surface in different orientations. The top figure shows an exposed orientation of the Fabs that enables high antigen binding capacity. Middle figure shows a mixed orientation resulting in intermediate antigen binding and the lowest figure shows an inverse, hidden orientation of the Fabs providing only poor antigen binding.

This section has discussed sensor surfaces and methods for immobilization on QCM sensors. Two dimensional SAM surfaces have been proven as highly functional sensor surfaces when combined with optimised preparation and immobilization protocols. Essential criteria for biosensor surfaces such as reproducible immobilization levels, retained biological activity on the surface, low non-specific binding and ability to regenerate the surfaces have been successfully fulfilled.

6 Improving acoustic biosensors (Paper V-X)

Increasing the sensitivity of the sensor is a frequent objective for research and development within the sensor area. In biosensing, the objective is motivated by requirements to detect smaller molecular species, or lower concentrations than previously possible. In this section, three broadly different approaches to increase the sensitivity of acoustic biosensors will be examined and discussed. First, an approach to increase the effective sensitivity of a biosensor system by improving the mass transport capability of the sensor fluidics is investigated (Paper V and VI). Secondly, the use of polymers on QCM sensor surfaces to enhance the sensor response is evaluated (Paper VII and VIII). Last, thin film acoustic sensors with two orders of magnitude higher frequency is studied in view of its operation for biosensing (Paper IX). In addition, the ability to improve biosensing by combined measurement of frequency and motional resistance data is investigated for biomolecular interactions in Paper X.

6.1 Improved flow cells for QCM (Paper V-VI)

The crystals typically chosen for biosensing applications have large circular electrodes since the operation of the crystal in liquid sets high demands on the crystal performance and the high Q of these crystals have traditionally been preferred. The flow cells in which the crystal operates are designed with respect to the electrode since the walls of the flow cell should not interfere with the oscillations of the crystal. In studies of biomolecular interaction kinetics large flow cells will cause unattractive flow conditions that may limit the sensor performance. An approach to improve the fluidics of a QCM biosensor by modifying quartz crystal electrodes to fit a flow cell with better hydrodynamic properties was investigated in Paper V and VI.

Standard and modified quartz crystal resonators with corresponding flow cells were compared by flow simulations and experimental studies with an antibody-antigen interaction system. Figure 6.1 displays the studied quartz crystal resonators. The circular electrode has a diameter of 4.5 mm and the rectangular the dimensions of 1×4 mm.

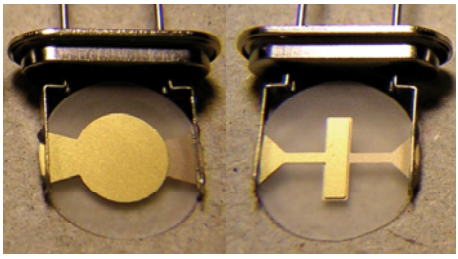

Figure 6.1. Images of the circular and modified rectangular quartz crystal electrodes.

The flow conditions of the corresponding flow cells with slightly larger dimensions than the respective electrodes were simulated in two dimensions, resulting in the flow velocity profiles presented in Figure 6.2. The flow velocity of the rectangular cell is essentially uniformly parabolic for the length of the flow cell, whereas in the circular cell the flow velocity decreases towards the widest section of the flow cell. As indicated by the lengths of the arrows for the respective flow cells, the flow velocity in the rectangular flow cell is significantly higher (3 times higher in the center of the flow cell), than in the circular flow cell. This results in a significantly thinner stagnant layer at the surface for the rectangular electrode and, consequently, in improved transport of sample to the sensor surface.

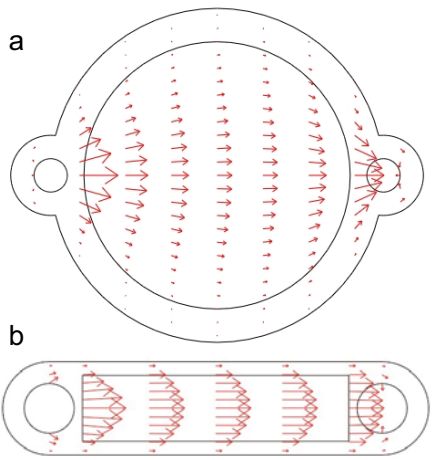

Figure 6.2. Linear velocity field profiles in the sensor chambers for circular a) and rectangular b) geometries. The inner boundary structures illustrate the respective sensor areas.

Experimental tests with antibody-antigen interaction system on the rectangular and circular flow systems revealed a higher responsiveness of the rectangular sensor at low concentrations as shown in Figure 6.3. The increase in response is consistent with a higher mass transport rate for the rectangular system as given by the higher flow velocity in that system. The higher noise

level observed for the rectangular system is indicative of the challenges that are involved in using modified, smaller electrodes in liquid sensor systems. As a result of the increased noise level, it is not certain that the detection limit, in terms of the signal-to-noise, will actually improve for sensor systems with small sensor electrodes if the increase in noise cannot be dealt with effectively. The improvement in mass transport characteristics as well as reduced dispersion in the flow cells are of significant importance for biomolecular interaction studies, particularly for interactions with fast reaction rates. This should motivate continued development of sensor electrode and flow cell geometries.

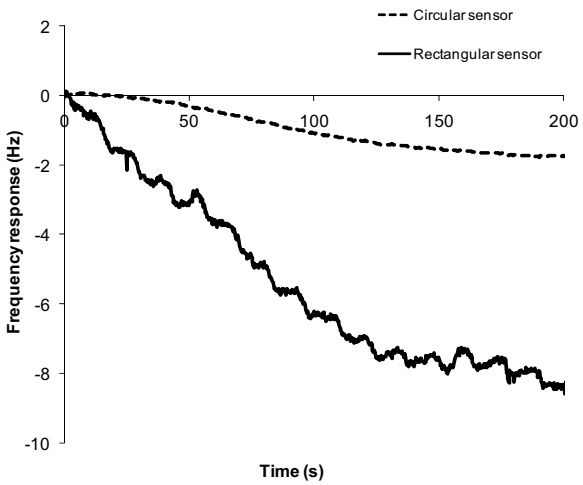

Figure 6.3. Sensor response of the rectangular (solid line) and circular (dashed line) sensor systems upon injection of 3.3 nM of a polyclonal anti-BSA antibody over BSA surfaces.

6.2 Polymers on QCM (Paper VIII-IX)

The magnitude of the sensor responses and consequently the sensitivity of a biomolecular interaction assay will often be dependent on the amount of biomolecules that can be immobilized on the sensor surface. In particular, this will be the case when the immobilized molecule is a protein receptor and the free analyte is a small molecular ligand such as those traditionally searched for in pharmaceuticals development. Pharmaceutical substances that can be orally administered often have a molecular weight of 500 Da or less. The respective receptor, immobilized on the sensor surface to allow for comparison between several different ligands, normally has a molecular weight of several 10000 Da. For instance, the ligand binding domains of the estrogen receptor are in the range of 30000 Da, whereas the molecular weight of the relevant agonist and antagonist ligands range from 200-500 Da

[36]. If such a receptor is immobilized on a biosensor surface at a level of 100 arbitrary units, the corresponding response from the ligand would be in the range of 1 arbitrary unit. This unfavorable leverage means that the amount of immobilized receptors needs to be high, in order to obtain a reasonable response level for the ligand. For two dimensional surfaces the amount of immobilized receptors will be limited to a full monolayer, which may still be insufficient. However, both optical sensors, such as SPR sensors, and acoustic sensors, such as QCMs, have the ability to sense events occurring in a volume over the surface given by the decay functions of the evanescent or acoustic field, respectively. The decay lengths for both QCM and SPR predict that events occurring within a few 100 nm will be sensed by the transducers. To accomplish immobilization in this domain over the sensor surface, hydrophilic polymers such dextran has been used successfully together with SPR, which has resulted in significantly increased immobilization levels and the ability to study small molecule receptor interactions [36,37]. For QCM sensors, the use of polymeric sensor surfaces to increase the immobilization and response levels has only been scarcely studied, and with limited success [38].

In Paper VII-VIII the potential of using polymeric surfaces on QCM sensors for increased response levels was assessed. Acryl amide/acrylic acid-polymer brushes were synthesized *in situ* on QCM substrates. The preparation of the surface first involved a coating of the QCM substrates with a polystyrene-like polymer film that contained photo initiator iniferter groups. The photo initiator iniferter acts as initiator, transfer agent and terminator during polymerization and allows for excellent control of the polymerization process. Specifically, it allows for control of the polymer thickness, which is essential for synthesis of polymeric sensor surface that need a defined thickness. Second, the iniferter coated substrates were immersed in monomer solutions containing acrylic acid and/or acryl amide polymers and was irradiated by UV light for the desired length of polymerization. A schematic for the immobilization process is shown in Figure 6.4.

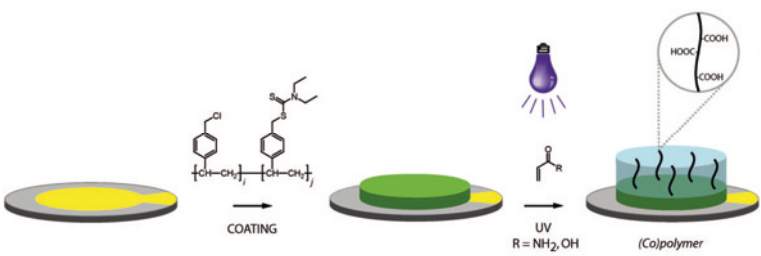

Figure 6.4. Surface preparation method for acrylic acid and acryl amide polymer brushes on QCM sensor surface.

The responsiveness of the synthesized QCM surfaces with respect to pH changes was investigated in Paper VII. The frequency responses of an acryl amide/acrylic acid copolymer is shown in Figure 6.5 for injections ranging from pH 3 to pH 9 (the running buffer adjusted to pH 3). Since the corresponding frequency responses for a grafted acrylamide polymer were significantly smaller and did not exhibit any pH dependence, the responses can be interpreted as a result of deprotonation of included carboxyl groups at higher pH. Deprotonation will cause charge repulsion within the polymer matrix, which results in an expansion of the polymer. When the polymer expands, more water will be sensed by the QCM, thereby resulting in the observed strong frequency responses. These dynamic responses of the sensor surface is indicative of the complexity of using polymers on QCM sensors, but also demonstrate that polymers can be used for enhancement of the sensor signal on QCM.

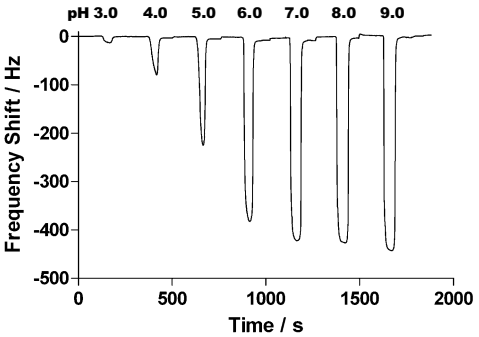

Figure 6.5. Frequency responses of polymer-coated QCM-crystals to injections of PBS of pH ranging from 3.0 to 9.0. The copolymer was grafted from a monomer solution with 9:1 of acryl amide to acrylic acid ratio.

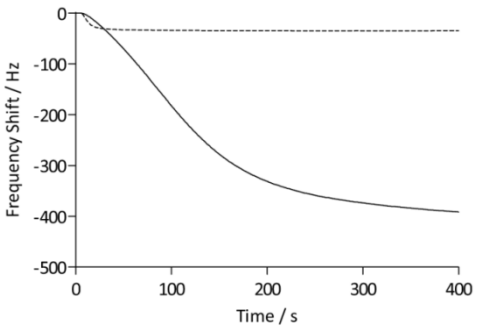

Figure 6.6. Protein binding analysis with biotin-presenting QCM surfaces. Frequency responses are shown for anti-biotin Fab (25 μg·mL^{-1}) binding to a biotin-derivatized pAAc surface (—) and to a biotin-derivatized carboxyl-terminated SAM surface (---).

To examine if the surface-grafted acrylic acid polymer (pAAc) could increase the response signal of a QCM, a biotin derivative, (+)-biotin-$(PEO)_4$ amine, was immobilized on the polymeric surface and on carboxyl SAM surfaces in Paper VIII. The interaction with an anti-biotin Fab-fragment was monitored as shown in Figure 6.6. The maximum response of the anti-biotin Fab fragments on the SAM surface was 35 Hz, compared to 390 Hz for the pAAc surface. Control injections on surfaces without immobilized biotin resulted in only minor responses. Evidently, the use of pAAc brushes results in a significant increase in the signal with more than 10 times higher response than for a carboxylated SAM surface. The three-dimensional nature of the matrix, in combination with potential dynamic effects, thus results in strong signal enhancement. Also, the initial rate of binding appeared slower for the pAAc surface compared to the carboxyl-terminated SAM surface. This behavior is most likely due to mass-transport phenomena in the polymer-based matrix, where, for example, the diffusion rate is expected to be lower for a particle moving in a matrix than for a free moving particle that adsorbs to a surface. The binding curves for the pAAc matrix also appear to be slightly sigmoidal. This could stem from the fact that the sensing capability, as given by the decay in displacement amplitude, is lowest at the top domains of the pAAc matrix. As previously discussed, the lateral displacement amplitude decays exponentially for a quartz crystal in a liquid medium. This means that the same number of molecules gives rise to a higher response if they are sensed closer to the surface of the quartz crystal, and that changes in liquid viscosity and density may affect the sensing performance of the quartz crystal. Since the sensitivity is highest at the shortest distance to the surface of the QCM electrode, gradual response shifts are expected over the matrix. The sigmoidal characteristic of the binding can thus be interpreted as the initial population of protein molecules binds at the top domain, giving rise to a smaller response, whereas subsequent penetration and binding of the matrix gives rise to a higher response.

The presented data shows that sensor responses of a QCM crystal with a polymer sensor surface are complex and are non-trivial in its interpretation. For instance, sensor responses due to changes in polymer viscosity and coupling of water to the polymer may occur, in addition to the commonly experienced aspects of bulk responses and coupling of water to protein adlayers [11]. Also, if material is bound to the surface the wave will propagate in a different manner in the adlayer than in the liquid, resulting in a change in oscillation frequency and the local amplitude distribution. Consequently, different adlayers may expand the sensing range of the sensor beyond the characteristic decay length and/or provide a larger frequency response than expected from the molecular mass. In an effort to gain better understanding of the viscoelastic aspects of protein binding to the sensor surfaces, motional resistance was measured concurrently with the frequency for the binding of anti-biotin Fab fragments. The change in resistance divided by the change in

frequency, ΔR/ΔF, can be used as measure of the viscoelastic contribution to the observed frequency change [39]. The ΔR/ΔF ratio for a anti-biotin Fab fragment binding to the carboxyl-terminated SAM surface was 3.7 mΩ/Hz whereas the ratio was 10 mΩ/Hz for the pAAc surface. Thus, the pAAc surface show approximately three times higher viscoelastic contribution to the frequency response than the carboxyl-terminated SAM surface. This confirms the expected response characteristics when proteins bound to the pAAc polymer is less rigidly attached to the crystal surface than those bound to SAM sensor surface.

Despite the complexity in data interpretation, it appears that polymeric coatings can be used to increase the signal responses of QCM sensors. More than tenfold increases in signal levels has been observed, which may be very helpful for studies of interactions between receptors and low molecular weight ligands.

6.3 Increasing the frequency – FBAR (Paper VII)

The mass sensitivity of a piezoelectric resonator is highly dependent to the resonance frequency. The Sauerbrey equation indicates a square relationship between the frequency responses from adsorbed mass and the fundamental resonance frequency [2]. This has been a driving force to make higher frequency resonators for sensor applications. Higher frequency can be obtained by making thinner resonators, or by using materials with higher shear wave velocity. Thinner quartz crystals have been investigated for the purpose of increasing the sensitivity. Resonators with fundamental frequency of 56 MHz were found to have the highest signal-to-noise ratio, whereas even higher frequencies resulted in disproportionate increases in signal noise that overshadowed the gained signal increase [40]. Recently, aluminum nitride (AlN) resonators made by thin film deposition processes has been demonstrated for liquid applications [41,42]. The shear velocity of AlN is significantly higher than for quartz, which will result in a correspondingly higher resonance frequency. Also, the thin techniques used for deposition of the AlN film makes it possible to make resonators with micro meter thickness as part of complex silicon structures. Figure 6.7 shows a thin film bulk acoustic resonator (FBAR) integrated in a flow cell. The 2 μm tilted AlN film is equipped with electrodes on each side and the surrounding silicon constitutes the physical structure that support the resonator and the flow cell. The fundamental resonance frequency of devices such as this one is in the range of 1-2 GHz which is a 100 to 200 times increase compared to the 10 MHz quartz crystal resonators discussed in this thesis. The increased fundamental frequency results in responses that are increased by a factor of 1000-4000 for an 800 MHz FBAR in an immunosensor application [41]. The theoretical increase would be larger, 6400, but the difference could be explained by

different flow conditions in the respective setups leading to non-similar mass transport rates to the sensor surface. Also, frequency dependence in viscosity and elasticity parameters as well as in the amount of hydrodynamically coupled water may impact the experienced frequency shifts.

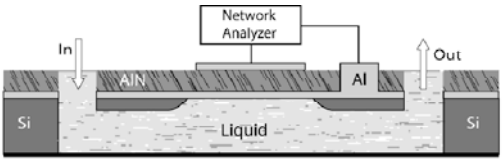

Figure 6.7. Thin film bulk acoustic resonator and flow cell in cross section.

The increased frequency also has the consequence that the decay of the wave in liquid will be faster. The theoretical decay length for a FBAR operating at 0.8 GHz would be 20 nm, which is only around four times the dimension of streptavidin, a protein commonly used in bioanalytical assays [43]. In Paper IX, the impact of wave decay on the effective sensing range of a FBAR is investigated. An FBAR sensor surface was coated with alternating layers of streptavidin (SA) and biotinylated bovine serum albumin (bt-BSA). A total of 90 alternating layers of SA and bt-BSA were coated onto an 800 MHz FBAR as shown in Figure 6.8. For the first 20 SA/bt-BSA double layers, the frequency shifts are consistently negative. At around 20 double layers of SA/bt-BSA the frequency shift for subsequent injections turns positive until around 40 layers where the resonance frequency becomes insensitive to deposition of additional layers. The reversed frequency shift is the result of film resonance, due to constructive interference of the waves inside the low impedance protein film [44]. The reversed frequency shift occurs at around quarter a wavelength of a thick viscoelastic film, which here corresponds to a thickness of around 200 nm, based on a thickness for the protein double layer of 10 nm [45]. Beyond this thickness, additional protein layers results in positive frequency shifts, instead of negative and it is therefore important to be aware of this aspect when working with thick polymer films. The linear responsiveness of the FBAR sensor up to 20 double layers, indicates that the sensor will be suitable for biosensor applications since most biosensor assays involve only a few protein layers. The strong future potential of FBARs in biosensing lies in harvesting the higher intrinsic sensitivity by addressing the higher noise level in these devices. In addition, the manufacturing process allow for production of these devices at low cost and in arrays of sensors which may be useful for higher through-put biosensor operation.

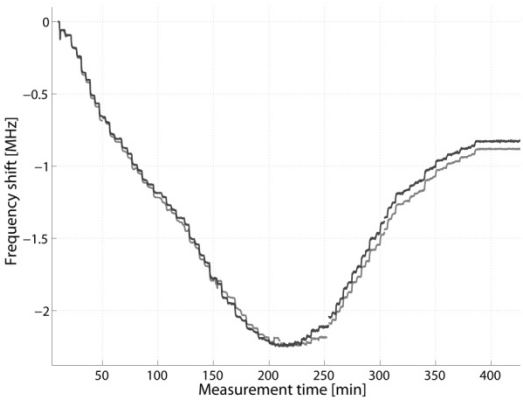

Figure 6.8. Frequency shifts from 90 alternating injections of streptavidin and biotinylated BSA to an 800MHz FBAR. The two curves correspond to series and parallel resonance.

6.4 Resistance measurements (Paper X)

Compared to optical techniques such as SPR, which can measure the concentration of immobilized or bound species at a given time, the QCM also has the advantage of providing information on the structure and conformation of the molecules on the surface by means of dissipation, amplitude or motional resistance measurements [8,11,12,14,46,47]. Specifically, QCM has previously been demonstrated to be a versatile tool for surface science and related applications because of its combination of frequency and dissipation measurements [16,48-51]. Dissipation measurements have been used to asses adlayer viscosity and conformational change, which has provided valuable insights on, for instance, protein adsorption to various surfaces. The dissipative characteristics between biomolecules vary significantly and could depend on rigidity of the molecular structure, hydrophobicity of exposed surfaces and mode of attachment to the sensor surface. The dissipative characteristics of immobilized proteins and DNA, as a function of the immobilization load of the respective molecules, was investigated in Paper X. Resistance data, in relation to frequency data, are shown in Figure 6.9. Glycerol samples, which provide purely viscous load to the sensor, have the highest ΔR to Δf relationship. Immobilized DNA shows lower resistance per frequency unit than glycerol, but higher than the two proteins. The high degree of the ΔR to Δf ratio for DNA has been shown to correlate with a high degree of viscoelasticity and large amount of coupled water for these films. This has contributed to the interest in dissipation monitoring of DNA [11,14,15,47,52,53].

The relationship between resistance and frequency data for DNA is found to be almost linear, especially in limited frequency ranges. In an overall trend, however, the ratio between the resistance and the frequency appears to decrease as the surface approaches saturation. This pattern can be interpreted as a lower water entrapment per immobilized DNA molecule for densely packed films. Also, increased electrostatic repulsion at higher surface densities has been suggested to reduce DNA strand flexibility making the surface more rigid [47]. However, it should be pointed out that an expected continuous increase of the viscoelastic parameters per added molecule in a film not necessarily results in linearity of the ΔR/Δf plots. Semicircular dependence of the real part (ΔR) versus the imaginary part (correlated to Δf) of the change in acoustic impedance has been observed during the cross-linking of polymer films [54]. Any conclusions based on the correlation between curvature and conformational changes in the biological layers should therefore be carefully treated. Regardless, the curvature and slope of ΔR over Δf is in any case dependent on the properties of the adlayer and it can consequently be used for comparative studies between various films.

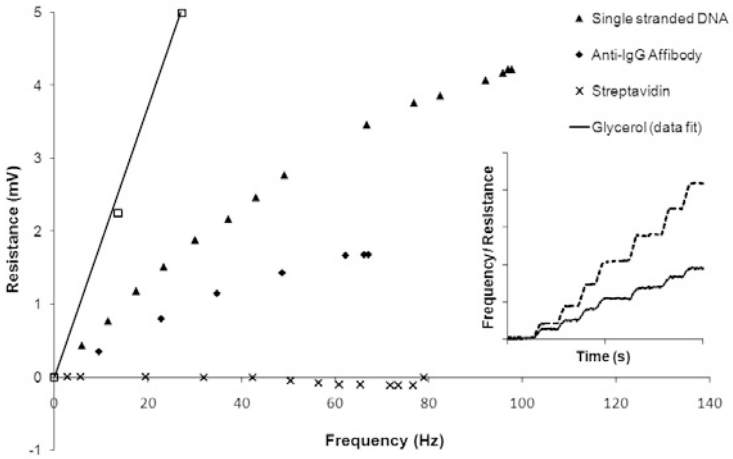

Figure 6.9. Frequency and resistance data for glycerol (empty squares), single stranded 40-mer biotinylated DNA (filled triangles), biotinylated anti-IgG Affibody (filled diamonds) and streptavidin (crosses). Inset shows real-time frequency (dashed line) and resistance (solid line) interaction data for binding of biotinylated DNA to a streptavidin surface. The biotinylated DNA was titrated onto the surface to provide careful readings of the frequency and resistance shifts.

The ΔR/Δf characteristics for proteins can be widely different: Titration of streptavidin onto a biotinylated sensor surface shows virtually no response in the resistance as shown by the data points along the x-axis of Figure 6.9. Alternatively, proteins can exhibit dissipative characteristics similar to DNA. Titration of biotinylated anti-IgG Affibody, a 14.6 kDa protein derived from

Protein A, onto a streptavidin coated sensor surface displays a $\Delta R/\Delta f$ ratio of about half of the DNA surface and with a similar trend regarding $\Delta R/\Delta f$ decreases at high surface concentrations.

The absence of resistance response for the streptavidin film indicates that proteins can form very rigid surfaces. One could speculate that the mode of attachment to the surface is of importance for the observed rigidity. While the biotinylated Affibody will be attached via only one flexible biotinylated linker to the rigid streptavidin surface, the streptavidin should theoretically have the possibility to be attached in two sites to the biotinylated surface. Comparative studies with streptavidin and anti-IgG Affibody covalently attached by amine coupling to a carboxyl surface, however, showed very similar results to the biotinylated samples with very low resistance responses for streptavidin. This indicates that the respective protein structures, including availability and distribution of primary amino groups, play an important role in defining the dissipative characteristics of the formed films.

In interaction studies, monitored increases in dissipation during adlayer formation or molecular binding events correspond to increased energy losses from the QCM sensor. These increased losses can be due to (i) added viscoelastic load by biomolecular binding to the surface, (ii) increased viscous load due to introduction of sample in viscous medium often referred to as bulk response, (iii) increased losses within the adlayers or (iv) increased losses from the interface between adlayer and bulk liquid. While the changes in viscous load due to changes in bulk liquid properties often can be reduced or eliminated by careful sample preparation the other three causes of energy losses are more difficult to control independently. Binding of biomolecules to the surface will inevitably result in viscous losses since these binding events are, with a few exceptions, non-rigid [11,15]. Consequently, binding to the surface will result in a frequency shift and a change in resistance. Also, certain protein interactions are known to involve large conformational changes in the protein structures in conjunction with complex formation [55]. If a binding event is associated with a change in conformation of the adlayer that increases the internal or interfacial energy loss, the change in the monitored resistance during the binding event will increase. If the binding event can be described by a first association event and a second conformational change event, and these occur with the same kinetic rates, the frequency and the resistance signals will have the same kinetic content. If, hypothetically, the first association event is faster than the conformational change event, the frequency and resistance data may have different time dependence. In such case, separate determination of kinetic rate constants from frequency and resistance data, could provide additional information on the binding event and improve the understanding of complex biomolecular binding and, potentially, the structural-functional relationship.

To assess the potential for reaction rate determination of biological events with a QCM sensor equipped to provide both real-time frequency and

motional resistance data, the interaction of a monoclonal anti-human serum albumin antibody (anti-HSA) with human serum albumin (HSA) was studied. Figure 6.10 shows the interaction data after double referencing according to Myszka [56].

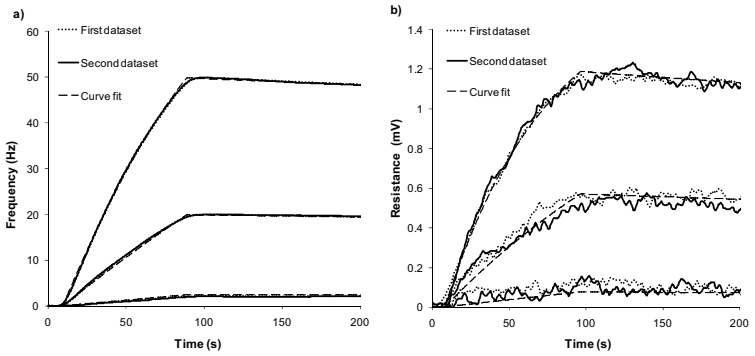

Figure 6.10. Duplicate frequency (a) and resistance (b) data set for interactions between immobilized anti-HSA and HSA at concentrations 1.5, 14 and 41 nM. Frequency data was globally fitted to a 1:1 model with mass transport compensation. The association rate was determined to $5*10^5$ M^1s^{-1} and the dissociation was determined to $4*10^{-4}$ s^{-1}, whereas the mass transport rate was found to be $3.8*10^7$ M^1s^{-1}.

Frequency data for the interaction was fitted to a 1:1 binding model with ClampXP Data Analysis Software [26], using compensation for mass transport limitations with the two compartment model. The good agreement between experimental data (dotted and solid line) and numerical fit (dashed line) shows that the QCM sensor can be used for studies of kinetic binding events and that the model system agrees with a 1:1 interaction model. Also, the almost two order of magnitude larger mass transport rate than association rate confirm that mass transport limitations in the presented data set will have a limited impact on the determined reaction rates. Visual inspection of the resistance data (see Figure 6.10b) reveals broadly similar characteristics in the resistance data as in the frequency data, except for the significantly higher noise level in the resistance signal. A global data fit on the resistance data using a 1:1 model, shows an association rate that was decreased by 40% compared to the frequency data and an off-rate that was essentially the same. While one of the incentives to carry out resistance measurement is to acquire additional and non-redundant information on the binding events, and potentially be able to determine complex binding events that occur in different steps with different rates, the data presented here shows a distinctive difference in association rates. Before arriving at the conclusion that, indeed, different binding and conformational change phases are observed in the presented data, the previously discussed phenomenon of decreased $\Delta R/\Delta f$ ratio for increased surface concentration need to be addressed.

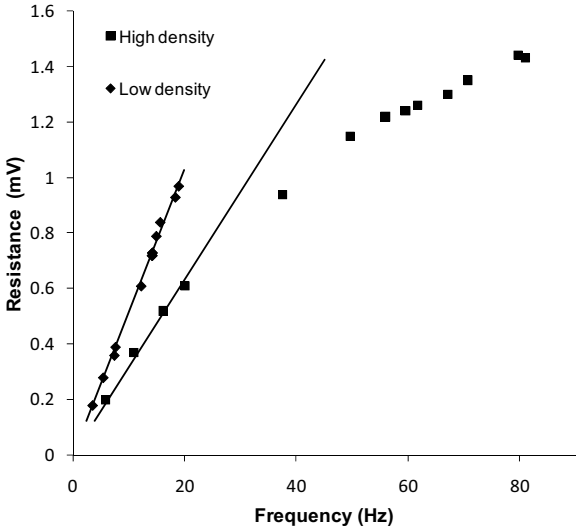

Figure 6.11. Frequency and resistance data for HSA binding data to low (filled diamonds) and high (filled squares) density surfaces of immobilized anti-HSA.

Examination of the relationship between ΔR and Δf for HSA to anti-HSA at high and low density of immobilized anti-HSA is shown in Figure 6.11. Samples of HSA were titrated onto the surfaces in a stepwise manner until saturation was reached. The data show that the relationship between ΔR and Δf is linear for the low density surface until its saturation at approximately 20 Hz. For the high density surface, a nice linear fit could be obtained for the first four data points, which was in the same frequency range as the low density surface. The data points above 20 Hz showed a significant deviation from the linear characteristics. Consequently, the likely interpretation of the kinetics data set for the anti-HSA to HSA interaction is that the lower association rate observed in the resistance data is due to increased rigidity in the layer at higher anti-HSA surface densities. To resolve potential conformational change events that occur at a different rate than the localization, a maximum surface density of less than 20 Hz would be recommended for this particular interaction system. In turn this is challenging the possibility to obtain the resistance data with sufficient signal to noise ratio, since a lower frequency response generally is accompanied by a lower resistance response. On the other hand, less dense surfaces provide binding data with higher ΔR to Δf ratios as shown by higher slope of the low density data set compared to the high density data set of Figure 6.11. This relationship can be utilized to obtain resistance data of suitable quality even for low density sensor surfaces. In summary, resistance measurements has the potential to complement frequency data for biomolecular interaction studies and as such, be a useful tool for increasing the understanding of complex binding events.

7 Findings and future prospects

This thesis has focused on the development of electroacoustic sensors, such as QCM and thin film bulk acoustic resonators, for biomolecular interaction studies. A QCM biosensor system with continuous flow and controlled sample injection was developed and proven for both affinity determination and kinetic analysis. Preparation methods for SAM based sensor surfaces were optimized and shown to provide highly functional biosensor surfaces. Versatile immobilization methods were developed that allowed for immobilization of very acidic biomolecules onto carboxyl surfaces, either by an optimized immobilization protocol using an EDC/sulfo-NHS reagent or by use of an externally applied electric field. The EDC/sulfo-NHS method was demonstrated for a panel of antibodies with high reproducibility, and detailed studies of the pH dependence in immobilization level and antigen binding capacity revealed that antibody orientation on two dimensional carboxyl surfaces could be highly dependent on immobilization pH. The use of an external electric field to immobilize biomolecules is instrumentally more demanding, but in return allows for greater chemical flexibility on the sensor surface. For instance, sensor surfaces with very low concentration of charges on the surface can be used since the attractive force can be provided by the electric field. Also, the ability to manipulate protein transport and binding in a biosensor system could be useful not only for immobilization of other strongly charged biomolecules, such as nucleic acids and carbohydrates, but could, speculatively, be of benefit for the regeneration of sensor surfaces during subsequent steps in the biosensor assay.

Efforts were made to improve the effective sensitivity of QCM sensors by use of modified, smaller quartz crystal electrodes that were designed to fit more optimized flow cells. The study revealed that the mass transport to the sensor surface could be significantly increased, which is valuable for resolution of fast kinetic rates. The smaller crystals exhibited an improved response level, however, accompanied by a higher noise level thereby limiting the improvement in signal-to-noise. If the increased noise can be addressed by improved design of the flow system or by numerical noise reduction, higher sensitivity and better kinetic resolution can be harvested. The reduced dispersion that would be gained should also be beneficial for serial connection of QCM flow through sensors and potentially QCM array sensor systems.

The use of polymeric sensor surfaces was explored to examine if higher immobilization and response levels could be obtained with the three dimensional characteristics of surface grafted polymer brushes. The carboxylated polymer brushes proved functional as sensor surfaces by tests with a Fab fragment-antigen model system. Compared with two dimensional sensor surfaces, the response level was increased more than ten-fold. This suggests that polymeric surfaces on QCM crystals could be advantageous for demanding applications, such as small molecule-receptor interaction assays. The signal responses from polymeric surfaces on QCM sensors exhibit similar characteristics as observed for SPR based sensors, with diffusion limitations within the polymer and decreasing sensitivity with increasing distance from the sensor surface. Added complexity exists for QCM sensors since the response from protein binding is not only dependent on the mass of the bound molecule, but also on the viscoelasticity of its attachment to the sensor as well as the amount of water that is sensed together with the molecule. Given this complexity, additional studies of polymeric sensor surfaces on QCMs are necessary to determine the relationship between the frequency response and surface concentration, since knowledge of this relationship is important for accurate kinetic studies. Also, significant challenges remain in finding the optimal polymer composition for QCM sensors in order to realize the full potential of this concept.

Higher frequencies of resonating devices have been predicted to result in higher sensitivity to adsorbed mass and a faster decay of the acoustic wave from the sensing surface. The impact of the decreased decay length of thin film bulk acoustic resonators operating in the GHz range on biomolecular interaction studies was investigated. Layer-by-layer deposition of proteins on the FBAR sensor showed linear responsiveness for up to 20 double layers of proteins, which suggests that this sensor will be suitable for biomolecular interaction studies and immunosensor use as most biosensor assays involve only a few protein layers. Further work on FBAR sensors is motivated, since successful reduction of the higher noise level currently experienced with these devices would lead to significant increases in effective sensitivity. Also, the rapid decay of the wave in the liquid could be beneficial for analysis of samples in complex biological media, such as serum and plasma, since a smaller fraction of the bulk liquid is probed by the FBAR sensor compared to the QCM. The relative impact of responses from changes in bulk medium should therefore decrease in favor of binding events to the sensor surface for these devices. Additional potential for FBAR sensors is given by the microstructure manufacturing methods that should allow for volume production of these sensors at relatively low cost and for fabrication of sensor arrays, to be used for higher throughput biosensor operation and diagnostic screening.

QCM sensors have the ability to provide information on the viscoelasticity of adlayers by means of dissipation or motional resistance measurements. A setup for combined frequency and motional resistance measurements was

developed and was found to provide data in agreement with previously published reports. Studies of protein and DNA immobilization showed that proteins can exhibit both viscoelastic and completely rigid binding characteristics. The ratio between differential resistance and frequency was found to decrease at higher surface concentrations of both DNA and proteins, which can be interpreted as increased surface rigidity at higher surface concentrations of immobilized molecules. Also, in interaction studies between antibodies and proteins, higher surface concentrations of interacting molecules led to a decrease in the differential resistance to frequency ratio. Consequently, studies that aim at obtaining biological binding information from resistance or dissipation data should be conducted at low surface concentrations. In addition, the differential resistance to frequency relationship was found to be highly dependent on the rigidity of the preceding layer(s) of immobilized molecules. While the study showed that the developed setup had suitable resolution for determination of kinetic rate constants, both based on frequency and resistance data, additional studies of biologically relevant interaction systems are necessary to elucidate the full potential of combined frequency and resistance measurements. Studies of protein interaction systems, which are well known to involve large conformational changes during the binding event, would be of particular interest to determine if these conformational changes could be specifically detected by the resistance measurements. In such a case, separate determination of kinetic rate constants from frequency and resistance data, could provide additional information on the binding event and improve the understanding of complex biomolecular binding and, potentially, the structural-functional relationship.

8 Sammanfattning på svenska

Interaktioner mellan livets byggstenar såsom proteiner, kolhydrater och nukleinsyror styr alla levande organismers existens. Studier för att förstå dessa interaktioner kräver olika typer av verktyg. Biosensorer är analysinstrument som medger studier av dessa interaktioner i realtid. Vanligtvis sätts en viss typ av molekyler fast på en sensoryta, till exempel en receptor, och en annan molekyl, en ligand, flödas över ytan. Sensorytan är en del av en mycket känslig sensor och när liganden binder till receptorn på ytan ger detta upphov till en elektrisk signal. Sensorn som omvandlar den biokemiska signalen till en elektrisk signal kan vara baserad på optiska eller akustiska detektionsprinciper. Akustiska sensorer med frekvenser utanför det hörbara området (20-20000 Hz) används bland annat för ekolod (~200 kHz), och för medicinska ultraljudsundersökningar (~2- 13 MHz). Vid högre frekvenser minskar vågens utbredning från sensorn och mindre objekt kan avkännas. I denna avhandling har akustiska sensorer med frekvenser på 10 MHz eller högre, så kallade QCM-sensorer studerats. En QCM sensor består av en kvartskristallplatta med motstående elektroder på vardera sida. Eftersom kvarts är piezoelektriskt kan en akustisk våg skapas i materialet med hjälp av en pålagd växelspänning, och en stående våg uppstår. En av kristallplattans elektroder exponeras för provvätska med hjälp av en flödescell, och när material fastnar på denna elektrod förändras den akustiska vågen, vilket detekteras som en minskning i en uppmätt resonansfrekvens. Genom att mäta resonansfrekvensens förändring när en ligand flödas över en inbunden receptor ges en uppfattning om hur stark bindningen mellan de båda är, och bindningsstyrkan eller den så kallade affiniteten kan bestämmas. Om det också undersöks med vilken hastighet liganden och receptorn binder till och lossnar från varandra kan de så kallade kinetiska reaktionshastigheterna mellan de båda bestämmans.

I detta arbete har ett mikroanalytiskt QCM-system med kontinuerligt flöde och väldefinierad provinförsel utvecklats för att kunna bestämma bindningskinetik och affinitet mellan biomolekyler. För att utvärdera systemets prestanda utvecklades en metod för relativ affinitetsbestämning mellan kolhydrater och kolhydratbindande proteiner, så kallade lektiner. Metoden uppvisade data som överensstämde väl med tidigare publicerade data, erhållna med hjälp av andra bioanalytiska metoder.

Infästning av molekyler, eller immobilisering, kräver väldefinierade sensorytor och reproducerbara immobiliseringsmetoder. Tre olika studier av

sensorytor och metoder för immobilisering av biomolekyler på sensorytor har undersökts i detta arbete. En metod för framställning av sensorytor baserad på självorganiserande filmer med kemiskt aktiverbara karboxylgrupper har optimerats. Med hjälp av denna metod kunde väldefinierade sensorytor framställas som visades ha mycket goda funktionella egenskaper när de användes tillsammans med de QCM-baserade biosensorerna. För att kunna immobilisera väldigt sura biomolekyler utvecklades ett instrument där sensorytan och flödescellen kunde exponeras för ett elektriskt fält. Med hjälp av det elektriska fältet kunde en sur peptid, C-peptid, immobiliseras på en karboxylerad sensoryta, vilket tidigare inte varit möjligt. Vidare optimerades en generell metod för antikroppsimmobilisering på karboxylerade sensorytor. Mängden immobiliserad antikropp och antigensinbindning som funktion av pH under immobiliseringen studerades i detalj och orienteringen av antikroppen på sensorytan visade sig vara kraftigt beroende av immobiliserings-pH för en av de studerade antikropparna. Metoden uppvisade hög reproducerbarhet i immobiliseringsnivåerna för en testpanel av antikroppar och medgav också immobilisering vid låga pH.

En rad studier har genomförts i detta arbete för att öka känsligheten hos de akustiska sensorerna. QCM-sensorer med små sensorelektroder kombinerades med en förbättrad flödescell för att öka transporten av biomolekyler till sensorytan och därmed förbättra den effektiva känsligheten. Denna uppställning gav en väsentlig ökning i responssignalen tack vare den mer effektiva transporten till sensorn, vilket är värdefullt för kinetiska studier av snabba molekylinteraktioner. Vidare undersöktes om användning av sensorytor med tredimensionella polymerer kunde användas för immobilisering av fler molekyler per ytenhet och därigenom förbättra känsligheten hos sensorn. Interaktionsstudier mellan ett immobiliserat antigen och ett antikroppsfragment visade att signalen kunde ökas mer än tio gånger jämfört med tvådimensionella sensorytor. Eftersom högre frekvenser hos akustiska sensorer har förutsetts ge högre känslighet så har också tunnfilmsresonatorer med cirka hundra gånger högre frekvenser än QCM sensorerna undersökts med avseende på biosensortillämpningar. Den högre frekvensen medför ett väsentligt mindre avkänningsområde från sensorytan, vilket skulle kunna innebära en begränsing för dessa sensorers tillämpning. Emellertid, visade det sig att det linjära avkänningsområdet var mer än tillräckligt för de flesta biosensortillämpningar, såsom mätning av antigen-antikroppsinteraktioner. Slutligen utvecklades en uppställning för kombinerad mätning av resonansfrekvens och energiförluster, svängningsresistans, från sensorn. Denna uppställning visade sig leverera data som överrensstämde väl med tidigare publicerade arbeten. Tidsupplösta data, både gällande frekvens och svängningsresistans, kunde användas för att bestämma kinetiska parametrar för ett interaktionspar. Framtida studier med kombinerade frekvens- och resistansmätningar kommer förhoppningsvis kunna bidra till bättre förståelse av komplexa molekylinteraktioner och i förlängningen även ge en starkare koppling mellan funk-

tionell och strukturell karaktärisering av biomolekylär bindning. Med en bättre, mer detaljerad förståelse för kroppens biomolekylära interaktioner ökar möjligheten att förstå sjukdomar, och att utarbeta behandlingar för att lindra dessa.

9 References

[1] E. Gizelli, C.R. Lowe, Biomolecular sensors, Taylor & Francis, London, 2002.

[2] G. Sauerbrey, Verwendung von schwingquarzen zur wagung dunner schichten und zur mikrowagung, Z. Phys. 155 (1959) 206-222.

[3] P.L. Konash, G.J. Bastiaans, Piezoelectric-crystals as detectors in liquid-chromatography, Anal. Chem. 52 (1980) 1929-1931.

[4] T. Nomura, Single-drop method for determination of cyanide in solution with a piezoelectric quartz crystal, Analytica Chimica Acta 124 (1981) 81-84.

[5] K.K. Kanazawa, J.G. Gordon, Frequency of a quartz microbalance in contact with liquid, Anal. Chem. 57 (1985) 1770-1771.

[6] M. Thompson, C.L. Arthur, G.K. Dhaliwal, Liquid-phase piezoelectric and acoustic transmission studies of interfacial immunochemistry, Anal. Chem. 58 (1986) 1206-1209.

[7] M. Muratsugu, F. Ohta, Y. Miya, T. Hosokawa, S. Kurosawa, N. Kamo, H. Ikeda, Quartz crystal microbalance for the detection of microgram quantities of human serum albumin: Relationship between the frequency change and the mass of protein adsorbed, Anal. Chem. 65 (1993) 2933-2937.

[8] M. Rodahl, F. Hook, A. Krozer, P. Brzezinski, B. Kasemo, Quartz-crystal microbalance setup for frequency and Q-factor measurements in gaseous and liquid environments, Rev. Sci. Instrum. 66 (1995) 3924-3930.

[9] M. Rodahl, On the frequency and q factor response of the quartz crystal microbalance to liquid overlayers, Department of Applied Physics, Chalmers University of Technology, Göteborg, 1995, pp. 39.

[10] J.D.S. Ballantine, S.J. Martin, A.J. Ricco, G.C. Frye, H. Wohltjen, R.M. White, E.T. Zellers, Acoustic wave sensors and responses, Acoustic wave sensors, Academic Press, Burlington, 1997, pp. 36-149.

[11] F. Hook, B. Kasemo, The QCM-D technique for probing biomolecular recognition reactions. in: C. Steinem, and A. Janshoff, (Eds.), Piezoelectric sensors, Springer, Berlin 2006.

[12] C.G. Marxer, M.C. Coen, H. Bissig, U.F. Greber, L. Schlapbach, Simultaneous measurement of the maximum oscillation amplitude and the transient decay time constant of the qcm reveals stiffness changes of the adlayer, Analytical and Bioanalytical Chemistry 377 (2003) 570-577.

[13] K.K. Kanazawa, J.G. Gordon, The oscillation frequency of a quartz resonator in contact with a liquid, Analytica Chimica Acta 175 (1985) 99-105.

[14] A. Tsortos, G. Papadakis, E. Gizeli, Shear acoustic wave biosensor for detecting DNA intrinsic viscosity and conformation: A study with QCM-D, Biosens. Bioelectron. 24 (2008) 836-841.

[15] X. Su, Y.-J. Wu, W. Knoll, Comparison of surface plasmon resonance spectroscopy and quartz crystal microbalance techniques for studying DNA assembly and hybridization, Biosens. Bioelectron. 21 (2005) 719-726.
[16] E. Reimhult, C. Larsson, B. Kasemo, F. Hook, Simultaneous surface plasmon resonance and quartz crystal microbalance with dissipation monitoring measurements of biomolecular adsorption events involving structural transformations and variations in coupled water, Anal. Chem. 76 (2004) 7211-7220.
[17] M.V. Voinova, M. Jonson, B. Kasemo, 'missing mass' effect in biosensor's qcm applications, Biosens. Bioelectron. 17 (2002) 835-841.
[18] M.V. Voinova, M. Rodahl, M. Jonson, B. Kasemo, Viscoelastic acoustic response of layered polymer films at fluid-solid interfaces: Continuum mechanics approach, Phys. Scr. 59 (1999) 391-396.
[19] J.D. Watson, F.H.C. Crick, The structure of DNA, Cold Spring Harbor Symp. Quant. Biol. 18 (1953) 123-131.
[20] T.E. Creighton, Proteins: Structures and molecular properties, W.H. Freeman and Company, New York, 1993.
[21] G. Schreiber, Protein-protein interactions. in: E. Gizelli, and C.R. Lowe, (Eds.), Biomolecular sensors, Taylor & Francis, London, 2002.
[22] B.M. Berg, J.L. Tymoczko, L. Stryer, Biochemistry, W. H. Freeman and Company, New York, 2002.
[23] N. Michael Green, W. Meir, A.B. Edward, [5] avidin and streptavidin, Methods in enzymology, Academic Press, 1990, pp. 51-67.
[24] T.A. Morton, D.G. Myszka, I.M. Chaiken, Interpreting complex binding kinetics from optical biosensors: A comparison of analysis by linearization, the integrated rate equation, and numerical integration, Anal. Biochem. 227 (1995) 176-185.
[25] D.G. Myszka, X. He, M. Dembo, T.A. Morton, B. Goldstein, Extending the range of rate constants available from biacore: Interpreting mass transport-influenced binding data, Biophysical Journal 75 (1998) 583-594.
[26] D.G. Myszka, T.A. Morton, Clamp (c): A biosensor kinetic data analysis program, Trends in Biochemical Sciences 23 (1998) 149-150.
[27] D.G. Myszka, Advanced biosensor workshops, 2007.
[28] J.C. Love, L.A. Estroff, J.K. Kriebel, R.G. Nuzzo, G.M. Whitesides, Self-assembled monolayers of thiolates on metals as a form of nanotechnology, Chemical Reviews 105 (2005) 1103-1169.
[29] F. Davis, S.P.J. Higson, Structured thin films as functional components within biosensors, Biosensors and Bioelectronics 21 (2005) 1-20.
[30] A. Ulman, Formation and structure of self-assembled monolayers, Chemical Reviews 96 (1996) 1533-1554.
[31] B. Johnsson, S. Löfås, G. Lindquist, Immobilization of proteins to a carboxymethyldextran-modified gold surface for biospecific interaction analysis in surface plasmon resonance sensors, Anal. Biochem. 198 (1991) 268-277.
[32] S. Lofas, B. Johnsson, A novel hydrogel matrix on gold surfaces in surface-plasmon resonance sensors for fast and efficient covalent immobilization of ligands, Journal of the Chemical Society-Chemical Communications (1990) 1526-1528.

[33] R. Arnold, W. Azzam, A. Terfort, C. Wöll, Preparation, modification, and crystallinity of aliphatic and aromatic carboxylic acid terminated self-assembled monolayers, Langmuir 18 (2002) 3980-3992.
[34] H. Wang, S. Chen, L. Li, S. Jiang, Improved method for the preparation of carboxylic acid and amine terminated self-assembled monolayers of alkanethiolates, Langmuir 21 (2005) 2633-2636.
[35] G. Dunér, Signal enhancement by dynamic polymers in quartz crystal microbalance applications, Organic Chemistry KTH, Stockholm, 2009.
[36] R.L. Rich, L.R. Hoth, K.F. Geoghegan, T.A. Brown, P.K. LeMotte, S.P. Simons, P. Hensley, D.G. Myszka, Kinetic analysis of estrogen receptor/ligand interactions, Proceedings of the National Academy of Sciences of the United States of America 99 (2002) 8562-8567.
[37] B. Johnsson, S. Lofas, G. Lindquist, Immobilization of proteins to a carboxymethyldextran-modified gold surface for biospecific interaction analysis in surface plasmon resonance sensors, Anal. Biochem. 198 (1991) 268-277.
[38] S. Storri, T. Santoni, M. Minunni, M. Mascini, Surface modifications for the development of piezoimmunosensors, Biosens. Bioelectron. 13 (1998) 347-357.
[39] R. Lucklum, C. Behling, P. Hauptmann, Role of mass accumulation and viscoelastic film properties for the response of acoustic-wave-based chemical sensors, Anal. Chem. 71 (1999) 2488-2496.
[40] E. Uttenthaler, M. Schraml, J. Mandel, S. Drost, Ultrasensitive quartz crystal microbalance sensors for detection of m13-phages in liquids, 6th World Congress on Biosensors (Biosensors 2000), San Diego, California, 2000, pp. 735-743.
[41] G. Wingqvist, J. Bjurstrom, A.C. Hellgren, I. Katardjiev, Immunosensor utilizing a shear mode thin film bulk acoustic sensor, 20th European Conference on Solid-State Transducers, Goteborg, SWEDEN, 2006, pp. 248-252.
[42] G. Wingqvist, J. Bjurstrom, L. Liljeholm, V. Yantchev, I. Katardjiev, Shear mode aln thin film electro-acoustic resonant sensor operation in viscous media, Sensor Actuat. B-Chem. 123 (2007) 466-473.
[43] T. Cassier, K. Lowack, G. Decher, Layer-by-layer assembled protein/polymer hybrid films: Nanoconstruction via specific recognition, Supramol. Sci. 5 (1998) 309-315.
[44] S.J. Martin, G.C. Frye, Polymer film characterization using quartz resonators. in: B.R. McAvoy, (Ed.), 1991 Ultrasonics Symp, I E E E, Lake Buena Vista, Fl, 1991, pp. 393-398.
[45] F. Hook, J. Voros, M. Rodahl, R. Kurrat, P. Boni, J.J. Ramsden, M. Textor, N.D. Spencer, P. Tengvall, J. Gold, B. Kasemo, A comparative study of protein adsorption on titanium oxide surfaces using in situ ellipsometry, optical waveguide lightmode spectroscopy, and quartz crystal microbalance/dissipation, Colloids and Surfaces B-Biointerfaces 24 (2002) 155-170.
[46] C.G. Marxer, A.C. Coen, L. Schlapbach, Study of adsorption and viscoelastic properties of proteins with a quartz crystal microbalance by measuring the oscillation amplitude, J. Colloid Interface Sci. 261 (2003) 291-298.
[47] K.M.M. Aung, X.N. Ho, X.D. Su, DNA assembly on streptavidin modified surface: A study using quartz crystal microbalance with dissipation or resistance measurements, Sensor Actuat. B-Chem. 131 (2008) 371-378.

[48] F. Hook, B. Kasemo, T. Nylander, C. Fant, K. Sott, H. Elwing, Variations in coupled water, viscoelastic properties, and film thickness of a mefp-1 protein film during adsorption and cross-linking: A quartz crystal microbalance with dissipation monitoring, ellipsometry, and surface plasmon resonance study, Anal. Chem. 73 (2001) 5796-5804.
[49] F. Hook, B. Kasemo, M. Grunze, S. Zauscher, Quantitative biological surface science: Challenges and recent advances, ACS Nano 2 (2008) 2428-2436.
[50] F. Hook, M. Rodahl, B. Kasemo, P. Brzezinski, Structural changes in hemoglobin during adsorption to solid surfaces: Effects of pH, ionic strength, and ligand binding, Proceedings of the National Academy of Sciences of the United States of America 95 (1998) 12271-12276.
[51] F. Hook, M. Rodahl, P. Brzezinski, B. Kasemo, Energy dissipation kinetics for protein and antibody-antigen adsorption under shear oscillation on a quartz crystal microbalance, Langmuir 14 (1998) 729-734.
[52] W.Y.X. Peh, E. Reimhult, H.F. Teh, J.S. Thomsen, X.D. Su, Understanding ligand binding effects on the conformation of estrogen receptor alpha-DNA complexes: A combinational quartz crystal microbalance with dissipation and surface plasmon resonance study, Biophysical Journal 92 (2007) 4415-4423.
[53] C. Larsson, M. Rodahl, F. Hook, Characterization of DNA immobilization and subsequent hybridization on a 2D arrangement of streptavidin on a biotin-modified lipid bilayer supported on SiO2, Anal. Chem. 75 (2003) 5080-5087.
[54] E.J. Calvo, R. Etchenique, P.N. Bartlett, K. Singhal, C. Santamaria, Quartz crystal impedance studies at 10 MHz of viscoelastic liquids and films, Meeting on Interactions of Acoustic Waves with Thin Films and Interfaces, Leicester, England, 1997, pp. 141-157.
[55] L. Lo Conte, C. Chothia, J. Janin, The atomic structure of protein-protein recognition sites, J. Mol. Biol. 285 (1999) 2177-2198.
[56] D.G. Myszka, Improving biosensor analysis, J. Mol. Recogn. 12 (1999) 279-284.

Acta Universitatis Upsaliensis

Digital Comprehensive Summaries of Uppsala Dissertations from the Faculty of Science and Technology 658

Editor: The Dean of the Faculty of Science and Technology

A doctoral dissertation from the Faculty of Science and Technology, Uppsala University, is usually a summary of a number of papers. A few copies of the complete dissertation are kept at major Swedish research libraries, while the summary alone is distributed internationally through the series Digital Comprehensive Summaries of Uppsala Dissertations from the Faculty of Science and Technology. (Prior to January, 2005, the series was published under the title "Comprehensive Summaries of Uppsala Dissertations from the Faculty of Science and Technology".)

Distribution: publications.uu.se
urn:nbn:se:uu:diva-107211

ACTA
UNIVERSITATIS
UPSALIENSIS
UPPSALA
2009